

國立交通大學

電機學院光電顯示科技產業研發碩士班

碩 士 論 文

低溫高介電係數材料於有機薄膜電晶體製程之研究

Study of Organic Thin Film Transistor with High-k Material
by Using Low-temperature Supercritical Technology

研 究 生：周 誼 明

指導教授：劉 柏 村 博士

中 華 民 國 九 十 七 年 一 月

低溫高介電係數材料於有機薄膜電晶體製程之研究
Study of Organic Thin Film Transistor with High-k Material
by Using Low-temperature Supercritical Technology

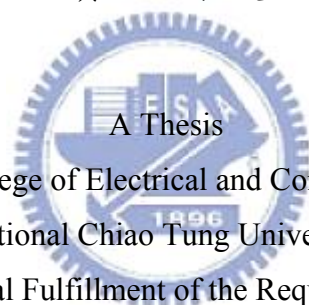
研 究 生：周誼明

Student：Yi-Ming Chou

指導教授：劉柏村

Advisor：Po-Tsun Liu

國立交通大學
電機學院光電顯示科技產業研發碩士班
碩 士 論 文



A Thesis

Submitted to College of Electrical and Computer Engineering
National Chiao Tung University
in partial Fulfillment of the Requirements
for the Degree of
Master
In

Industrial Technology R & D Master Program on
Photonics and Display Technologies

January 2008

Hsinchu, Taiwan, Republic of China

中華民國九十七年一月

低溫高介電係數材料於有機薄膜電晶體製程之研究

研究生：周誼明

指導教授：劉柏村

國立交通大學電機學院產業研發碩士班

摘 要

在此論文裡，我們研究了高介電常數材料與薄膜電晶體在超臨界二氧化碳流體混合水的熱處理下其電性的改變並將此高介電常數薄膜為絕緣層製造有機薄膜電晶體。首先，在室溫下，利用真空濺鍍系統成長極薄的氧化鉛薄膜，厚度約為 7 奈米，為了取代傳統的高溫退火製程，我們使用了溫度約 150°C 超臨界流體混合水的技術，為了驗證超臨界流體混合水能有效的使水分子進入到氧化鉛，進而減少薄膜的缺陷密度，我們經由紅外線光譜儀、熱脫附常壓游離質譜儀與 X 射線光電子能譜來做材料分析，結果均顯示於氧化鉛薄膜內氧的含量增加，而厚度為 7 奈米氧化鉛薄膜在閘極電壓 3 伏特的操作下，其單位面積漏電流約為 2×10^{-7} A/cm²，並且得到較高的崩潰電壓，崩潰電壓約為 24 伏特，傳導機制亦由原本未經處理的量子穿隧效應轉換為熱放射效應，以上主要的原因是由於氧化鉛薄膜的缺陷密度減少。

此外，我們利用經處理過的氧化鉛薄膜為絕緣層去製作有機薄膜電晶體，發現經由超臨界流體技術的處理之後，有機薄膜電晶體有較好的元件特性，其有機薄膜電晶體中的臨界電壓、場效移動率、次臨界擺幅和開關電流比例都有顯著的提升。這些改善主要是因為超臨界流體的技術，能有效修補懸鍵，進而減少氧化鉛絕緣層的缺陷密度。

由這些結果均顯示，藉由超臨界流體混合水的技術，能減少薄膜的缺陷密度。可預期的，若超臨界流體的特殊特性整合在高介電常數材料與有機薄膜電晶體，將具有其優勢。

Study of Organic Thin Film Transistor with High-k Material by Using Low-temperature Supercritical Technology

Student : Yi-Ming Chou

Advisor : Dr. Po-Tsun Liu

Industrial Technology R & D Master Program of
Electrical and Computer Engineering College
National Chiao Tung University

ABSTRACT

In this study, supercritical fluids (SCF) technology is employed originally to effectively improve the properties of low-temperature-deposited metal oxide dielectric films and fabricate organic silicon thin film transistors (OTFTs). In this work, 7 nm ultra-thin Hafnium Oxide (HfO_2) films are fabricated by sputtering method at room temperature, and replacing the conventional high temperature annealing with supercritical fluids treatment at 150 °C. The supercritical fluids act a transporter to deliver H_2O molecule into the HfO_2 films for repairing defect states. After this proposed process, the absorption peaks of Hf-O-Hf bonding apparently raise and the quantity of oxygen in HfO_2 film increases from FTIR and TDS measurement, individually. The leakage current density of 7 nm HfO_2 film is cut down to $2 \times 10^{-7} \text{ A/cm}^2$ at $|V_g| = 3 \text{ V}$, and the conduction mechanism is transferred from quantum tunneling to thermal emission because of the significantly reducing the defects in the HfO_2 film. Moreover, the higher breakdown voltage is obtained, reaching $|V_g| = 24 \text{ V}$.

Additionally, supercritical fluids technology is also proposed to effectively passivate the defect states in HfO_2 insulator of OTFTs at low temperature (150 °C). After the treatment of supercritical fluids mixed with water and propyl-alcohol, the characteristics of OTFTs are better.

This proposed technology is also used to improve the transfer characteristics of OTFTs at 150 °C. From theses experimental results, the better sub-threshold swing, lower off-current, higher on/off current ratio and higher mobility are obtained, such that the supercritical CO_2 treatment provide a novel method to enhance the transfer characteristics of Organic thin film transistors

誌 謝

首先由衷地感謝指導老師劉柏村博士在我進修碩士學位期間的指導、教誨和鼓勵，老師孜孜不倦的研究精神，使我獲益匪淺，不僅僅是在學術研究上的指導，對於人生規劃及待人處事的態度上，亦讓我獲益良多，僅在此獻上最誠摯的謝意。諸位口試委員的指導和建議，也在此謹申謝意。

此外，要感謝蔡志宗學長與楊柏宇學長悉心的教導使我得以一窺超臨界流體領域的深奧，尤其是蔡志宗學長在實驗、量測分析以及論文寫作給予我莫大的協助與建議，使我在這些年中獲益匪淺，順利獲得知識並取得學位。另外亦得特別感謝李逸哲學長、李昇翰學長、鄒一德學長、林俊文學長、李啟銘學長、葉唐豪學長、李崇維學長與鄭逸立學弟的大力協助，因為有你們的陪伴、幫忙及搞笑讓兩年的研究生生活變得多彩多姿。還有要感謝黃震鏢學長、吳興華學長、陳弘根學長、黃千睿學長、曾子怡學姐、陳又菁學姐、蕭秀娟學姐、鍾宛芳學姐、聶建名學長、卓立革學姐，感謝學長姐們平日對我的照顧以及研究上的建議。也要感謝實驗室一起工作的同學—高逸侑，以及學弟—鄭逸立、竹立煒、郭豫杰、張繼聖、蔡尚祐、陳思維、林威廷、陳巍方、王超駿、蘇智昱、鄧立峯、楊維哲、黃羿霖…等，感謝你們陪伴我共同走過這一段甜美的日子，讓我無論是在實驗中或是讀書時永遠充滿歡樂。還有要感謝我的好友—胡智勇、許顯斌與潘俊六，感謝你們在我求學的路上一路相挺。同時，衷心感謝國家奈米元件實驗室(NDL)和交大半導體中心提供良好的研究設備與充分的資源。相當慶幸自己在研究期間有如此多的貴人相助，要感謝的人太多太多，無法一一列出，謹奉上最真心的感激與祝福。

最後，我願將這份榮耀呈獻給我深愛最後，我願將這份榮耀呈獻給我深愛的父母親—周豐年先生、盧娟娜女士。感謝父母親多年來辛苦的教導與栽培，一直在背後默默地支持與關懷我，陪我度過了許多風雨與榮耀的時光，讓我能無後顧之憂，全力衝刺學業，終於不負所望完成學業，在此獻上我內心最深的謝意。此外，特別要感謝陪伴我多年的女友—許嘉倩，在背後的默默支持更是我前進的動力，碩士班兩年因為妳的支持及協助，使我能順利的完成碩士學位，在此由衷的對妳說聲謝謝。

周誼明 2008年1月

Contents

Chinese Abstract	i
English Abstract	ii
Chinese Acknowledgment	iii
Contents	iv
Table Captions	vi
Figure Captions	vii
 Chapter 1 Introduction	
1.1 Introduction of Organic Thin-Film Transistors (OTFTs)	1
1.2 Metal Oxide dielectric films (High dielectric constant material, High-k)	2
1.3 Supercritical Fluid Technology	2
1.4 Motivation.....	3
 Chapter 2 Experiment Procedures and Principle	
2.1 Fabrication of Metal-Insulator-Silicon (MIS) and Experiment Process.....	5
2.2 Fabrication of (OTFTs) and Experiment Process.....	6
2.3 Properties of Organic Thin Film Transistors	
2.3.1 Characteristics of the organic materials.....	7
2.3.2 Operation of OTFTs	9
2.3.3 Transportation Mechanisms	11
2.3.4 Parameters extraction	13

Chapter 3 Analysis and Result

3.1 Thin Film Analysis of Electrical Characteristics and Discussion

3.1.1 The current density-electric field (J - E) characteristics	15
3.1.2 Conduction Mechanism.....	15
3.1.3 The capacitance-voltage (C - V) characteristics.....	20
3.1.4 Breakdown voltage measurement and gate bias stress.....	22

3.2 Thin Film Analysis of Material and Discussion

3.2.1 Fourier Trans-form Infrared Spectroscopy (FTIR) Analysis.....	24
3.2.2 Thermal Desorption System – Atmospheric Pressure Ionization Mass Spectrometer (TDS-APIMS) Analysis.....	25
3.2.3 X-ray Photoelectron Spectroscopy (XPS) Analysis.....	25
3.2.4 Transmission Electron Microscopy (TEM) Analysis.....	26

3.3 OTFTs Analysis of Electrical Characteristics and Discussion

3.3.1 The current density-electric field (J - E) characteristics.....	27
3.3.2 The capacitance-voltage (C - V) characteristics.....	28
3.3.3 Secondary Ions Mass Spectrometer (SIMS) Analysis.....	29
3.3.4 The current-voltage (I - V) characteristics.....	30
3.3.5 The DC bias and current stress characteristics.....	31

3.4 Summary.....

Chapter 4 Conclusion34

References63

Table Captions

Chapter 1

Table 1-1 Critical temperature and pressure for some common fluids..... 36

Table 1-2 Comparison of physical properties of CO₂..... 36

Chapter 2

Table 3-1 The extracted parameters from C-V curves of HfO₂ films after different treatment, measuring at 1M Hz with gate bias swing from negative voltage to positive voltage (forward). The V_{fb} means the flat-band voltage, and defined as $C/C_{max} = 50\%$. The change of flat-band voltage of different- treated HfO₂ films under forward swing is label as ΔV 62



Figure Captions

Chapter 1

Fig. 1-1 Phase diagram for CO₂..... 35

Fig. 1-2 Density-pressure-temperature surface for pure CO₂. 35

Chapter 2

Fig. 2-1 The supercritical fluid system. 37

Fig. 2-2 The experiment processes of thin HfO₂ film with various treatments.... 38

Fig. 2-3 The experiment processes of OTFTs with HfO₂ film of various Treatments. 39

Fig. 2-4 The energy band diagram of entacene. The optical energy gap and adiabatic energy gap are determined. 40

Fig. 2-5 Energy band diagrams (a) for a p-channel (pentacene) and (b) for a n-channel (NTCDA) OTFT. The left side shows the devices at zero gate bias, while in the centre and in the right parts the accumulation and depletion mode operation regimes are presented. 40

Chapter3

Fig. 3-1 The leakage current densities of HfO₂ films after different treatments (The negative bias is applied on gate electrode). 41

Fig. 3-2 Conduction mechanism for Al/HfO₂/Si MIS structure. 41

Fig. 3-3 (a) Curve of $\ln (J/E)$ versus reciprocal of electric field ($1/E$) for the baking-only treated HfO₂ film, and a schematic energy band diagram accounting for trap-assisted tunneling shown in the inset. (b) Leakage current density versus the square root of electric field ($E^{1/2}$) plot for the

	3000 psi-SCCO ₂ treated HfO ₂ film. The inset shows the energy band diagram of Schottky-type conduction mechanism.	42
Fig. 3-4	The leakage current densities of HfO ₂ films after different treatments (The positive bias is applied on gate electrode).	43
Fig. 3-5	The capacitance-voltage characteristics of HfO ₂ films after different treatment, measuring at 1M Hz with gate bias swing from negative voltage to positive voltage (forward) and from positive voltage to negative voltage (reverse).	43
Fig. 3-6	The mechanism of extracting of fixed charge with SCCO ₂ fluids.	44
Fig. 3-7	The equivalent capacitance models of MOS structure (a) without C _{it} , (b) with C _{it}	45
Fig. 3-8	The capacitance-voltage characteristics of HfO ₂ films after different treatment, measuring at 1M Hz and 100k Hz with forward gate bias swing.	45
Fig. 3-9	The breakdown characteristic curves of HfO ₂ films after various treatments (a) at positive and (b) at negative gate bias region, individually.	46
Fig. 3-10	The variation of leakage current of different-treated HfO ₂ films as a function of stress time at a high electric field = 5 MV/cm.	47
Fig. 3-11	The FTIR spectra of HfO ₂ films after various post-treatments, including Baking-only, H ₂ O vapor and 3000psi-SCCO ₂ treatment.	47
Fig. 3-12	The transporting mechanism for SCCO ₂ fluids taking H ₂ O molecule into HfO ₂ film.	48

Fig. 3-13	The thermal desorption spectroscopy (TDS) measurement, (a) m/e (mass-to-charge ratio) = 32 peak that is attributed to O_2 , (b) $m/e = 18$ peak that is attributed to CO_2	49
Fig. 3-14	The X-ray photoemission spectra of HfO_2 films O 1s after various post-treatments, including (a) Baking-only, (b) H_2O vapor and (c) 3000psi-SCCO ₂ treatment.	50
Fig. 3-15	The TEM images show the MIS (Al/ HfO_2 /Si-Substrate) structure after various post-treatments: (a) Baking-only treatment (b) H_2O vapor treatment and (c) 3000psi-SCCO ₂ treatment.	51
Fig. 3-16	The leakage current densities of HfO_2 films after different treatments.	52
Fig. 3-17	The capacitance-voltage characteristics of HfO_2 films after different treatment, measuring at 1M Hz with gate bias swing from negative voltage to positive voltage (forward) and from positive voltage to negative voltage (reverse).	52
Fig. 3-17	Secondary ion mass spectroscopy: (a) Si atom (b) Hf atom and (c) O atom in HfO_2 film of Baking-only and 3000 psi-SCCO ₂ treatment	53
Fig. 3-18	Current vs Voltage plots (I_D - V_G) characteristics of HfO_2 film: (a) Baking-only treatment and (b) H_2O vapor treatment. (OTFTs deposited on HfO_2 film with 3000 psi-SCCO ₂ treatment).	54
Fig. 3-19	Current vs Voltage plots (I_D - V_G) characteristics: (a) HfO_2 film of 3000 psi-SCCO ₂ treatment and (b) PECVD SiO_2 film.	55
Fig. 3-20	Current vs Voltage plots (I_D - V_D) characteristics: (a) HfO_2 film with 3000 psi-SCCO ₂ treatment and (b) PECVD SiO_2 film.	56
Fig. 3-21	Normailzed Current vs Voltage plots (I_D - V_D) characteristics of HfO_2 film	

	with 3000 psi-SCCO ₂ treatment and PECVD SiO ₂ film.	57
Fig. 3-22	Current vs Voltage (I_G - V_D) characteristics of a OTFTs deposited on HfO ₂ film with 3000 psi-SCCO ₂ treatment : (a) DC bias stress of $V_G = -20V$, (b) DC bias stress of $V_G = -20V$ and $V_D = -20V$ and (c) DC bias stress of $V_G = -20V$ and current stress of $V_D = -200nA$	58
Fig. 3-23	Mobility shift vs. bias stress time for DC bias stress of $V_G = -20V$, DC bias stress of $V_G = -20V$ and $V_D = -20V$ and DC bias stress of $V_G = -20V$ and current stress of $V_D = -200nA$ (OTFTs deposited on HfO ₂ film with 3000 psi-SCCO ₂ treatment).	59
Fig. 3-24	Threshold voltage shift vs. bias stress time for DC bias stress of $V_G = -20V$, DC bias stress of $V_G = -20V$ and $V_D = -20V$ and DC bias stress of $V_G = -20V$ and current stress of $V_D = -200nA$ (OTFTs deposited on HfO ₂ film with 3000 psi-SCCO ₂ treatment).	59
Fig. 3-25	Current vs Voltage (I_G - V_D) characteristics of a OTFTs deposited on PECVD SiO ₂ film : (a) DC bias stress of $V_G = -20V$, (b) DC bias stress of $V_G = -20V$ and $V_D = -20V$ and (c) DC bias stress of $V_G = -20V$ and current stress of $V_D = -200nA$	60
Fig. 3-26	Mobility shift vs. bias stress time for DC bias stress of $V_G = -20V$, DC bias stress of $V_G = -20V$ and $V_D = -20V$ and DC bias stress of $V_G = -20V$ and current stress of $V_D = -200nA$ (OTFTs deposited on PECVD SiO ₂ film)	61
Fig. 3-27	Threshold voltage shift vs. bias stress time for DC bias stress of $V_G = -20V$, DC bias stress of $V_G = -20V$ and $V_D = -20V$ and DC bias stress of $V_G = -20V$ and current stress of $V_D = -200nA$ (OTFTs deposited on PECVD SiO ₂ film).	61

Chapter 1

Introduction

1.1 Introduction of Organic Thin-Film Transistors (OTFTs)

The concept of using organic materials as semiconductors layer in transistors are realized at least since the 1980s [1,2]. Latterly, the organic thin film transistors (OTFTs) are of interest for the fabrication of low-cost, simple process and flexible displays. The OTFTs performance has been improved in the past decade and comparable to the hydrogenated amorphous silicon transistors (a-Si:H TFT) [3]. To fabricate organic transistors on plastic substrate, it is essential to decrease the process temperature. Many researchers have proposed individual methods to fabricate the pentacene-transistors and the reported field-effect mobilities are in the range of $0.001 \sim 3\text{cm}^2/\text{V}\cdot\text{sec}$ [4]. However, the OTFTs still face several problems: low-temperature gate dielectrics, reliably simple processes and low-mobility etc. At these issues, a more convenient for gate dielectric must be surmount a major obstacle.

Lately, the high-capacitance gate dielectrics can be achieved by the two methods. One is reducing the gate-dielectric thickness [5], the other was using the high-k material as the gate-dielectrics [6]. In low temperature deposited process, the high-k materials may low dielectric strength and ascend high leakage current in the utilization of OTFTs. The pinhole may be another question when reducing the dielectric thickness. So, a new dielectric is provided with higher dielectric permittivity, controllable insulator thickness and to reduce leakage current. That will be improving the OTFTs.

1.2 Metal Oxide dielectric films (High dielectric constant material, High-k)

The Majority of metal oxide dielectric films, such as HfO_2 , Ta_2O_5 and Al_2O_3 , hold higher dielectric constant than thermal oxide(SiO_2), and studied to replace the gate dielectric layer for future generation CMOS devices because of the lower leakage current and thicker physics thickness than thermal oxide (SiO_2) under identical equivalent oxide thicknesses (EOT) [7, 8]. Additionally, due to the property of high dielectric constant, For thin film transistors, in pervious records, the use of low-temperature-deposited metal oxide films as gate dielectrics not only reduces the threshold voltage to near zero for pentacene and zinc oxide (ZnO) TFTs but also the thickness of the gate insulator to nanometer scale [9, 10]. For extending the application, the novel method to improve the quality of metal oxide films is necessary.



1.3 Supercritical Fluid Technology

Supercritical fluids technology is a novel low temperature trap-passivation technology. The technology is compounds above their critical temperatures and pressure, as shown in Fig 1-1 [11, 12]. The advantage of supercritical fluids for commercial applications is their unique combination of liquid-like and gas-like properties. The Table 1-1 shows critical temperature and pressure for some common fluids. CO_2 -based supercritical fluids are particularly attractive because CO_2 is nontoxic, nonflammable, obtain easily and lower price. Besides, its critical conditions are easily achievable with existing process equipment ($31\text{ }^\circ\text{C}$, $1072\text{ psi} = 72.8\text{ atm}$).

Figure 1-2 shows the density-pressure-temperature surface for pure CO_2 . It can be discovered that relatively small changes in temperature or pressure near the critical

point, resulting in large changes in density. Table 1-2 shows the comparison of several physical properties of typical liquid, vapor, and supercritical fluid state for CO₂. It could be seen that supercritical CO₂ (SCCO₂) fluids possesses liquid-like density, so that SCCO₂ fluids are analogous with light hydrocarbon to dissolve most solutes and own exceptional transport capability [13, 14]. Besides, SCCO₂ fluids hold gas-like characteristic due to their viscosity and surface tension are extremely low, it allows SCCO₂ fluids to keep fine diffusion capability and enter the nano-scale pores or spaces without damage. These properties are the reasons for SCCO₂ fluids to employ in many commercial applications, including the extraction of caffeine from coffee, fats from foods, and essential oils from plants for using in perfumes. Furthermore, in last years, many records are investigated with SCCO₂ fluids to apply in semiconductor fabrication, such as cleaning wafer and stripping photoresist, by means of its high mass transfer rates and infiltration capabilities [14-16].



1.4 Motivation

In recent records, Metal oxide dielectrics, such as HfO₂, Ta₂O₅, and Al₂O₃ have attracted much attention for memory cell capacitors and gate dielectric applications in the ultra large scale integration (ULSI) technology [7, 8]. Among several metal oxide film formation methods [7, 8, 17], in general, low-temperature technology is welcome due to a low thermal and low price process. Also, it is suitable for thin film transistor liquid crystal displays (TFT-LCDs) technology on the base of glass substrates or plastics. However, the low-temperature-deposited dielectric films perform inferior properties and larger current leakage due to numerous traps inside the metal oxide film [18, 19]. Hence, the low-temperature-deposited metal oxide film to reduce electrical traps by implementing a post-treatment process is needed. The supercritical

fluids technology has been applied to remove photoresist and impurity in integrated circuit (IC) fabrications [20]. It is also operative method to extract moisture from structures of nanoscale, such as porous dielectric-material and carbon nano-tube [21, 22]. By the liquid-like property, it is allowed for supercritical fluids to own fine transport capability [23]. Supercritical fluids, in addition, hold gas-like and high-pressure properties to efficiently diffuse into thin films with no damage. Here, these advantages would be adequately employed to passivate the defects in low-temperature-deposited metal oxide dielectric film at 150 °C.

In addition, OTFTs will extensively research in the flexible displays. The excellent transfer characteristics are thereby demanded, such as high mobility and lower threshold voltage. Especially, in recent years, the fabrication of OTFTs tends to being implemented at low temperature processes for cost down and comparable with plastic substrates (120~250 °C)[24, 25]. The performance of low-temperature process for OTFTs, however, due to the poor gate dielectrics with great quantity of defects is unsuitable for application to display technology, [26]. For improving electrical characteristics of OTFTs, it is necessary to passivate the defect-states in the gate dielectrics. Therefore, it is critical to develop a low-temperature traps passivation technology for extending the application of OTFTs. In this work, therefore, the supercritical fluids treatment is also proposed to effectively decrease the defects in the gate dielectrics of OTFTs at low temperature.

Chapter 2

Experiment Procedures and Principle

2.1 Fabrication of Metal-Insulator-Silicon and Experiment Process

At first experiment, a metal-oxide HfO_2 film layer was deposited on p-type (100) silicon wafers by reactive DC magnetron sputtering at room temperature under Ar/O_2 ambient. The thickness of as-deposited HfO_2 films was 7nm, which was measured by an ellipsometer system. Subsequently, the wafers with 7nm-thick HfO_2 film were split into three groups, and processed with different post-treatments to study the properties of low-temperature-deposited HfO_2 film. The first group labeled as Baking-only treatment, was designed as the control sample, and was only baked on a hot plate at 150 °C for 2 hrs. The second group labeled as H_2O vapor treatment, was immersed into a pure H_2O vapor ambience at 150 °C for 2 hrs in a pressure-proof stainless steel chamber with a volume of 100cm³. The third sample marked as 3000psi- SCCO_2 treatment, was placed in the supercritical fluid system at 150°C for 2 hrs, where was injected with 3000psi of SCCO_2 fluids mixed with 5 vol.% of propyl alcohol and 5 vol.% of pure H_2O . The propyl alcohol plays a role of surfactant between nonpolar- SCCO_2 fluids and polar- H_2O molecules, so that the H_2O molecule uniformly distributes in SCCO_2 fluids and be delivered into the HfO_2 film for passivating defects. The supercritical fluid system is shown in Fig. 2-1.

After these different treatments, the thickness of HfO_2 films is almost intact, checked with the ellipsometer measurement. Fourier transformation infrared spectroscopy (FTIR) and thermal desorption spectroscopy (TDS) were also used to investigate the evolution of chemical functional bonding and the content of oxygen in HfO_2 films, respectively. Electrical measurements were conducted on metal insulator

semiconductor (MIS) capacitors by thermally evaporating Al electrodes on the front surface of the HfO_2 films and the backside of the silicon wafer. The current density-electric field (J - E) characteristics, capacitance-voltage (C - V) characteristics, breakdown voltage and gate bias stress were measured with HP4156C semiconductor parameter analyzer for investigating the transformation of HfO_2 film. The experiment processes of thin HfO_2 film with various treatments are exhibited in Fig. 2-2.

2.2 Fabrication of OTFTs and Experiment Process

At second experiment, a metal-oxide HfO_2 film layer was deposited on p-type (100) silicon wafers by E-beam thermally evaporating at room temperature. The thickness of as-deposited HfO_2 films was 150nm, which was measured by an ellipsometer system. Subsequently, the wafers with 150nm-thick HfO_2 film were split into three groups, and processed with different post-treatments to study the properties of low-temperature-deposited HfO_2 film. The first group labeled as Baking-only treatment, was designed as the control sample, and was only baked on a hot plate at 150 °C for 2 hrs. The second group labeled as H_2O vapor treatment, was immersed into a pure H_2O vapor ambience at 150 °C for 2 hrs in a pressure-proof stainless steel chamber with a volume of 100cm³. The third sample marked as 3000psi-SCCO₂ treatment, was placed in the supercritical fluid system at 150°C for 2 hrs, where was injected with 3000psi of SCCO₂ fluids mixed with 5 vol.% of propyl alcohol and 5 vol.% of pure H_2O . The propyl alcohol plays a role of surfactant between nonpolar-SCCO₂ fluids and polar- H_2O molecules, so that the H_2O molecule uniformly distributes in SCCO₂ fluids and be delivered into the HfO_2 film for passivating defects.

After these different treatments, The gate contact by thermally evaporating Al

electrodes on the backside surface of the silicon wafer. Then, the wafer was put into the oven with HMDS steam for 20mins at 150 degree. Pentacene was used as an active layer. This was deposited using ULVAC thermal evaporator. The deposition is started at a pressure lower than 3×10^{-6} torr. The deposition rate is controlled at 0.1 Å/s. The temperature we use in depositing pentacene films is 70°C. We use shadow mask to define the active region of each device. the resulting thickness of the pentacene thin film was 70 nm, which was measured by a quartz-crystal thin film thickness monitor. After pentacene deposition, We use shadow mask to define top contact of each device. The top electrodes are Au. We deposited the Au (100nm) via the thermal evaporator as the source and drain electrode pad. The deposition pressure was at 3×10^{-6} torr with the deposition rate of 0.5 Å/sec. In addition, we fabrication the same process to comparison with insulation of SiO₂ by Plasma Enhanced Chemical Vapor Deposition (PECVD).

After fabrication OTFTs, The current density-electric field (J - E) characteristics, capacitance-voltage (C - V) characteristics, Current-Voltage (I - V) characteristics, current stress and DC bias stress were measured with HP4156C semiconductor parameter analyzer for investigating the OTFTs. The experiment processes of OTFTs with various treatments are exhibited in Fig. 2-3.

2.3 Properties of Organic Thin Film Transistors

2.3.1 Characteristics of the organic materials

Organic conjugated materials can be generally sorted small molecules and polymers in OTFTs. The one single bond exhibit contiguous sequences of double bonds separated. The π orbital in the conjugated system is linked with the neighboring π orbital, and spreads in the whole molecule. The π electrons are delocalized across

the molecule, which makes conductive or semiconducting characteristics of the conjugated system. Unlike the case in inorganic semiconductors, the carrier transport is band-like transport which is determined by the Bloch wave states. Carrier transport is via hopping between localized states in disordered organic semiconductors.

Mobility is the most important parameter when we mention about OTFTs. The localized wave functions in organic semiconductors lead to small inter-molecular interactions, typically the weak π - π overlap or van der Waals. That is the main cause of the low mobility. But it can be improved by modifying the materials and device architectures. Pentacene is one of the most widely-used in OTFTs materials. Its mobility has reached the fundamental limit ($> 3 \text{ cm}^2/\text{Vs}$) [27,28] which is obtained with a single crystal at room temperature. Organic semiconductors are soluble in vaporizable or organic solvents at low temperatures due to such small inter-molecular interactions. This implies that there may be a trade-off between the mobility and processability in organic semiconductors of OTFTs. The mobility of organic semiconductors ranged from 0.001 to $3 \text{ cm}^2/\text{Vs}$ is comparable to that of amorphous silicon transistors which is widely developed and used in flexible displays.

First introduces the polymer material. Conjugated polymers are more suitable than small molecules for solution processability due to their high viscosity. However, the mobility of conjugated polymer is generally smaller than that of small molecule semiconductors for the more random orientation of molecular units or relatively short conjugated length in polymer backbones. The mobility as high as $0.1 \text{ cm}^2/\text{Vs}$ has been achieved with regioregular head-to-tail poly(3-hexylthiophene) [29]. More recently, it has been shown that the mobility can be raised to $0.2 \text{ cm}^2/\text{Vs}$ when the polymer film is applied by dip-coating to a thickness of only 2-4nm [30]. Polymer-based TFTs offer the advantage of spin-coating or inkjet printing, but in turn decreases the mobility, the

purity defects in material may give rise to charge-trapping sites.

In addition, introduces the small molecules material. Since the spin-coated polymer is disordered in structure, the structure of thermal evaporated small molecule is well ordered. Small molecules can be classified into linear fused ring compounds, 2-D fused ring compounds, oligomers, and 3-D molecules.

Most organic materials tend to transport holes better than electrons. This is because the OTFTs is p-type semiconductors are more stable in air and larger mobility. Most n-type organic semiconductors are sensitive to moisture and air due to the organic anions. Especially, the carbanions can easily react with water and oxygen under operating conditions, which causes the low mobility of n-type organic semiconductors.

Thereupon, we choose pentacene as material of the semiconductor region. Because pentacene material is have the largest mobility and more stability.

Pentacene is an aromatic compound with five condensed benzene rings, the chemical formula is $C_{22}H_{14}$ with molecular weight 278.3. The volume of the unit cell is about 705Å [31]. The permittivity is 4 [32], and the electron affinity is about 2.49eV. Silinish et al. determined the adiabatic energy gap (E_G^{Ad}) by using the threshold function of intrinsic photoconductivity of pentacene [33]. The second transition is from the excited state to the ionic state, which is called the optical energy gap (E_G^{Opt}). The energy band of pentacene are exhibited in Fig. 2.4 [34]

2.3.2 Operation of OTFTs

Organic thin-film transistors are basically similar to traditional thin-film transistors in structure. Two common device structures are used in organic TFTs. Although there is not large difference between inorganic TFTs and organic TFTs, the

operation modes of these two kinds of transistors are not the same at all.

Since pentacene is a p-type semiconductor. First, a negative bias is applied to the gate, the voltage drops over the insulator and semiconductor regions, which gives rise to band bending in the semiconductor. The additional positive charges provided by the source and drain electrodes accumulate charges in this region. The insulator serves as a capacitance which stores charges and can be represented as C_{OX} . It is assumed that a little voltage drop across the semiconductor is negligible. In this situation, the applied drain bias can direct the current from source to drain. The conduction is determined by mobility μ which represents how the electrical field drives the accumulated charges. Therefore, the increased gate voltage δV_G accounts for the increased charges $C_{OX}\delta V_G$ and the total charges increased over the channel are $WLC_{OX}\delta V_G$, where L and W correspond to the channel length and width. The increased drain current δI_D then represented as

$$\delta I_D \approx \frac{W}{L} C_{OX} \mu V_D \delta V_G \quad (2.1)$$

In general, we can divide the operation of OTFTs into two regions, linear and saturation regions. The drain current in the linear region is determined from the following equation

$$I_D = \frac{W}{L} C_{OX} \mu (V_G - V_{TH} - \frac{V_D}{2}) V_D \quad (2.2)$$

Since the drain voltage is quite small, sometimes equation (2.2) can be simplified as

$$I_D = \frac{W}{L} C_{OX} \mu (V_G - V_{TH}) V_D \quad (2.3)$$

For $-I_D > -(V_G - V_{TH})$, I_D tends to saturate due to the pinch-off of the accumulation layer. The current equation is modified as

$$I_D = \frac{W}{2L} C_{OX} \mu (V_G - V_{TH})^2 \quad (2.4)$$

The energy band diagrams for n-type and p-type OTFTs are shown in Fig. 2.5 [35].

2.3.3 Transportation Mechanisms

Latterly, two principal types of theoretical model are used to describe the transport in organic semiconductors : “The band-transport model” and “The hopping models”. Multiple trapping and release (MTR) model assumes that most of the carriers injected in the semiconductor are trapped in states localized in the forbidden gap. MTR model is widely used in amorphous silicon TFTs [36.37] and explains reasonably well the observed characteristics in vapor-deposited polycrystalline pentacene films. The model assumes that the intrinsic charge transport mechanism is the one involving extended states, and a distribution of traps exists in the forbidden gap above the valence-band edge. At low gate biases, most of the holes injected in the semiconductor are trapped into these localized states. The deepest traps are first filled and carriers can be thermally released. As the negative gate bias increases in p-type materials, the Fermi level approaches the valence-band edge and more traps are filled. At an appropriately high gate voltage, all trap states are filled and subsequently injected carriers move with the microscopic mobility in the delocalized (valence) band [38.39]. Several trap levels have been reported for polycrystalline vapor-deposited pentacene films at depths ranging from 0.06eV to 0.68eV [40], which can account for the MTR model. Traps are sometimes caused from the impurities and structure defects in the crystalline pentacene film which include dislocations, point defects and most importantly, the grain boundaries [41]. The concept of grain boundaries has been used to explain the gate-voltage dependence of mobility in polycrystalline oligothiophene

films [42,43]. The energy barrier created in the grain boundaries is a function of trapped charge states, carrier concentration within the grains and temperature.

At high temperatures, the charge transport is dominated by the thermionic emission over the potential barrier at grain boundaries. At low temperatures, the carrier transport is dominated by tunneling. However, mobility in molecular crystal is still moderate at very low temperatures. The corresponding mean free path does not exceed the inter-molecular distance, which is not physically acceptable for a diffusion-limited transport. Polaron models have been proposed to rationalize the discrepancy [44]. In spite of the recent efforts, the best explanation and exact phenomenon describing the carrier transport in molecular crystals are still under investigation.

The concept of variable range hopping (VRH) [45] is usually used in organic transistors, where the carriers transport by hopping: thermally activated carriers tunneling between localized states including percolation, rather than by the activation of carriers to a transport level.

The model describes the conductivity in the polymer as equivalent to transport through a resistor network. The percolation criterion through the network is then related to the temperature, the position of Fermi level, and the width of the exponential tail of the density of states.

A carrier may either hop over a long distance with low activation energy or hop over a small distance with high activation energy. As the accumulated charges fill the lower lying states, any additional charges will occupy states with relatively higher energy. Therefore, these additional charges just need less energy to hop away to neighboring sites, and the mobility will rise as the gate voltage increases.

2.3.4 Parameters extraction

In this section, we introduce four parameters are used to evaluate the performance of OTFTs. They are field effect mobility, threshold voltage, sub-threshold slope and on/off current ratio.

Mobility

Field effect carrier mobility is usually considered the most critical part of these four parameters. The behavior of an OTFT is revealed with the observation of carrier mobility. Mobility of an OTFT is affected by many factors, such as the trap density of active layer, ambient temperature, and carrier concentration. In OTFTs, the mobility mainly depends on the ordering of molecules and trap density.

Generally, mobility can be extracted from the trans-conductance in g_m the linear region :

$$g_m = \left[\frac{\partial I_D}{\partial V_G} \right]_{V_D = \text{CONSTANT}} = \frac{WC_{ox}}{L} \mu V_D \quad (2.5)$$

Mobility can also be extracted from the slope of the curve of the square-root of drain current versus gate voltage in the saturation region, i.e. $-V_D > -(V_G - V_{TH})$:

$$\sqrt{I_D} = \sqrt{\frac{W}{2L}} \mu C_{ox} (V_G - V_{TH}) \quad (2.6)$$

On/Off current ratio

Devices with high on/off current ratio represent ratio of the large turn-on current and small off current. It determines the gray-level switching of the displays. High on/off current ratio means there are enough turn-on current to drive the pixel and sufficiently the low current when the device is turned off.

Threshold voltage

Threshold voltage is related to the power consumptions and the operation voltage of OTFTs. Many researches on OTFTs are suffered from the large threshold voltage.

Threshold voltage is influenced by the ratio of the mobile and trapped carriers at the interface between the organic semiconductor layer and insulator. There are also researches on lowering the threshold voltage by adjusting the insulator layer [46]. In our experiments, we extract the threshold voltage from equation (2.6), the intersection point of the square-root of drain current versus gate voltage when the device is in saturation mode operation.

Sub-threshold Slope

Sub-threshold voltage is defined to evaluate the sensitivity of drain current to gate voltage in OTFTs. The following equation is used to define sub-threshold voltage. Obviously, a well-performed TFT will have a smaller value of sub-threshold voltage. This means that the relatively large swing of drain current can be achieved with a relatively small gate voltage.



Chapter 3

Analysis and Result

3.1 Thin Film Analysis of Electrical Characteristics and Discussion

3.1.1 The current density-electric field (J - E) characteristics

The leakage current densities of HfO₂ films after different treatments are shown as a function of applied negative gate bias voltage in Fig. 3-1. Among various post-treatments, the baking-treated HfO₂ film exhibits the most serious leakage current, inferentially due to its poor dielectric characteristics with numerous traps inside the HfO₂ film and the interface between parasitical SiO_x and Si wafer. The improvement of electrical characteristics is observed by using H₂O vapor process, however, a high leakage current density still appears at larger applied voltages. It could be inferred reasonably dependent on the defect passivation efficiency. The most indicating that H₂O vapor can passivate the traps (or defects) and alter dielectric properties of the low-temperature-deposited HfO₂ film. After H₂O vapor treatment, effective improvement of electrical characteristic is obtained by the 3000 psi-SCCO₂ treatment, exhibiting the lowest leakage current density among all samples. Low leakage current density ($\sim 2 \times 10^{-7}$ A/cm²) is kept constantly, even biased at an electric field of 3 MV/cm. The electrical performance agrees with FTIR analysis, in which 3000 psi-SCCO₂ treatment modified HfO₂ dielectrics even effectively.

3.1.2 Conduction Mechanism

There may be different conduction mechanisms in the insulator thin film, including Schottky-Richardson emission [47], Frenkel-Poole emission [47,48], Fowler-Nordheim tunneling [47,48], and trap assisted tunneling [49,50] illustrated in

Fig 3-2. The Schottky-Richardson emission generated by the thermionic effect is caused by the electron transport across the potential energy barrier via field-assisted lowering at a metal-insulator interface. The leakage current governed by the Schottky-Richardson emission is as following:

$$J_{SR} = A^* T^2 \exp\left(\beta_{SR} E^{1/2} - \phi_{SR}/k_B T\right) \quad (3.1)$$

where $\beta_{SR} = (q^3/4\pi\epsilon_0\epsilon)^{1/2}$, q is the electronic charge, A^* is the effective Richardson constant, ϕ_{SR} is the contact potential barrier, E is the applied electric field, ϵ_0 is the permittivity in vacuum, ϵ is the high frequency relative dielectric constant, T is the absolute temperature, and k_B is the Boltzmann constant. We can find the slope of the leakage current equation.

$$\ln J_{SR} = \beta_{SR} E^{1/2}/k_B T + [\ln(A^* T^2) - \phi_{SR}/k_B T] \quad (3.2)$$

$$\text{Solpe} = \beta_{SR}/k_B T \quad (3.3)$$

The Frenkel-Poole emission is due to field-enhanced thermal excitation of trapped electrons in the insulator into the conduction band. The leakage current equation is:

$$J_{FP} = J_0 \exp\left(\beta_{FP} E^{1/2} - \phi_{FP}/k_B T\right) \quad (3.4)$$

where $J_0 = \sigma_0 E$ is the low-field current density, σ_0 is the low-field conductivity, $\beta_{FP} = (q^3/\pi\epsilon_0\epsilon)^{1/2}$, q is the electronic charge, ϕ_{FP} is the contact potential barrier, E is the applied electric field, ϵ_0 is the permittivity in vacuum, ϵ is the high frequency relative dielectric constant, T is the absolute temperature, and k_B is the Boltzmann constant. We can find the slope of the leakage current equation.

$$\ln J_{FP} = \beta_{FP} E^{1/2} / k_B T + [\ln(J_0) - \phi_{FP} / k_B T] \quad (3.5)$$

$$Solpe = \beta_{FP} / k_B T \quad (3.6)$$

The Fowler-Nordheim tunneling is the flow of electrons through a triangular potential barrier. Tunneling is a quantum mechanical process similar to throwing a ball against a wall often results that the ball goes through the wall without damaging the wall or the ball. It also loses no energy during the tunnel event. The probability of this event happening, however, is extremely low, but an electron incident on a barrier typically several nm thick has a high probability of transmission. The Fowler-Nordheim tunneling current I_{FN} is given by the expression [51]:

$$I_{FN} = A_G A_{FN} \varepsilon_{ox}^2 \exp(-B_{FN} / \varepsilon_{ox}) \quad (3.7)$$

where the A_G is the gate area, ε_{ox} is the oxide electric field, and A_{FN} and B_{FN} are usually considered to be constant. A_{FN} and B_{FN} are given as the following:

$$A_{FN} = q^3 (m/m_{ox}) / 8\pi h \Phi_B = 1.54 \times 10^{-6} (m/m_{ox}) / \Phi_B \quad (3.8)$$

$$B_{FN} = 8\pi (2m_{ox} \Phi_B^3)^{1/2} / 3eh = 6.83 \times 10^7 [(m/m_{ox}) \Phi_B^3]^{1/2} \quad (3.9)$$

where m_{ox} is the effective electron mass in the oxide, m is the free electron mass, q is the electronic charge, and Φ_B is the barrier height at the silicon-oxide interface given in units of eV in the expression for B_{FN} . Φ_B is actually an effective barrier height that take into account barrier height lowering and quantization of electrons at the semiconductor surface. Rearranging I_{FN} formula gives by:

$$\ln(I_{FN} / A_G \varepsilon_{ox}^2) = \ln(J_{FN} / \varepsilon_{ox}^2) = \ln(A_{FN}) - B_{FN} / \varepsilon_{ox} \quad (3.10)$$

A plot of $\ln(J_{FN}/\epsilon_{ox}^2)$ versus $(1/\epsilon_{ox})$ should be a straight line if the conduction through the oxide is pure Fowler-Nordheim conduction [51].

In the trap assisted tunneling model, it is assumed that electrons first tunnel through the SiO_x interfacial layer (direct-tunneling). Then, electrons tunnel through traps located below the conduction band of the high-k thin film and leak to substrate finally [49]. The equation of leakage current density is [50]:

$$J = \alpha/E_{ox} \exp(-\beta/E_{ox}) \quad (3.11)$$

From the equations as shown above, leakage current behaviors of insulate films can be investigated further on the leakage current density J electric field E characteristics such as J vs. $E^{1/2}$ plots.

The plot of the nature log of leakage current density versus the square root of the applied electric field was observed. It is found that the leakage current density is linearly related to square root of the applied electric field. The linear variations of the current correspond either to Schottky-Richardson emission or to Frenkel-Poole conduction mechanism. For trap states with coulomb potentials, the expression is virtually identical to that of the Schottky-Richardson emission. The barrier height, however, is the depth of the trap potential well, and the quantity β_{FP} is larger than in the case of Schottky-Richardson emission by a factor of 2.

Leakage conduction mechanism is also investigated to support the comments on the electrical improvement of HfO₂ film. Fig. 3-3(a) plots $\ln(J/E)$ versus reciprocal of electric field variation for the baking-only treated HfO₂ film, and a schematic energy band diagram accounting for leakage transport mechanism shown in the inset. A good linear fitting explains Fowler-Nordheim (F-N) tunneling [52] occurs in the electric fields higher than 0.7 MV/cm. Also, it is consistent with the electrical behavior of

baking-only treated HfO₂ film in Fig. 3-1 that leakage current density sharply increases, while gate bias voltage larger than 0.7 MV/cm. This could be attributed to the trap-assisted tunneling due to numerous traps inside the 150°C- baking treated HfO₂ film [53]. For the 3000 psi-SCCO₂ treated HfO₂ film, a plot of leakage current density versus the square root of the applied field ($E^{1/2}$) gives a good representation of the leakage behavior at high electric fields, as shown in Fig. 3-3(b). The leakage current density of the 3000 psi-SCCO₂ treated HfO₂ is linearly related to the square root of the applied electric field, demonstrating Schottky-Richardson emission transport mechanism [54]. The Schottky-type conduction can be verified by comparing the theoretical value of $\beta_{SR} = (q^3 / 4\pi\epsilon_0\epsilon)^{1/2}$ with the calculated one obtained from the slope of the experimental curve $\ln J$ versus $E^{1/2}$ [55], where q is the electronic charge, ϵ_0 the dielectric constant of free space, ϵ is the high frequency relative dielectric constant. The Schottky emission generated by the thermionic effect is caused by electron transport across the potential energy barrier via field-assisted lowering at a metal-insulator interface, shown in the insert of Fig. 3-3(b), and independent of traps. From the slope of $\ln J$ versus $E^{1/2}$, the calculated value of relative dielectric constant (ϵ) is 26.4, and which is close to the determined value of 29.4 in capacitance-voltage ($C-V$) measurement (referring to table 3-1). This also proves, for 3000psi-SCCO₂ treated HfO₂ film, the conduction mechanism is really Schottky emission, but not trap-dependent Poole-Frenkel emission [55]. Additionally, the evolution of conduction mechanisms from trap-assisted tunneling to Schottky emission can confirm these defects inside low-temperature-deposited HfO₂ film is minimized effectively by implementing the proposed SCCO₂ technology. The leakage current densities of HfO₂ films after different treatments are shown as a function of applied positive gate bias voltage in Fig. 3-4, and the lower leakage current still could

be acquired after 3000 psi-SCCO₂ and H₂O vapor treatment, especially treated with SCCO₂ fluids. This could be attributed to the influence of traps in the interface between parasitical SiO_x and Si wafer. Generally, in positive gate bias, the sources of electron are (1) the interface states, (2) defects in depletion region, (3) back electrode of substrate, [56] and the later two source are negligible due to the p-type signal-crystal Si wafer is used in this work. For baking-only treated HfO₂ film, the great quantity of interface states still exist which generate electron-hole pair and lead to higher leakage current, as described in the inset of Fig. 3-4. After 3000 psi-SCCO₂ treatment, the interface states were deactivated, hence the leakage current is reduced. The reduction of interface states would be proved in capacitance-voltage measurement.

3.1.3 The capacitance-voltage (*C-V*) characteristics

The capacitance-voltage (*C-V*) characteristics are also generally used to judge the quality of dielectric films. Figure. 3-5 shows capacitance-voltage characteristics of HfO₂ films after different treatment, measuring at 1M Hz with gate bias swing from negative voltage to positive voltage (forward) and from positive voltage to negative voltage (reverse). The slope of *C-V* curve in transient region, i.e. from C_{\max} to C_{\min} , is relative to the interface states, for example, the sharp slope indicates fewer defects exist in the interface between HfO₂ and Si wafer. In Fig. 3-5, the baking-treated HfO₂ film presents the worst *C-V* curve and lower capacitance. This expresses the larger number of interface states exist and lead to the smooth *C-V* curve. Additionally, the lower dielectric constant, as shown in table 3-1, could be referred to the influence of defects in HfO₂ film. With H₂O vapor treatment, the sharper *C-V* curve and higher capacitance are obtained, and it could be attributed to the reduction of defects in HfO₂ film and the interface. Furthermore, the best improvement is achieved by 3000

psi-SCCO₂ treatment. This exhibits that the SCCO₂ treatment possesses excellent ability to passivate the defects, including Hf dangling bonds and interface states.

Besides, from Fig. 3-5, the shift of C-V curve under forward and reverse swing is also appears in baking-treated and H₂O vapor-treated HfO₂ films. It is resulted from the trapped carrier in defects of HfO₂ films, and that is not expected for gate insulator of transistors. Under negative gate bias, the electric inject from Al gate into HfO₂ films and trapped by defects, leading to the larger gate bias is required for inducing electron-inversion layer. For describing clear, we define the flat-band voltage is the gate bias as $C/C_{\max} = 50\%$, and the shift of the flat-band voltages under forward and reverse swing is shown in table 3-1. It is evidently observed that the baking-treated HfO₂ film hold numerous defects because of the extensive shift of flat-band voltage, and the defects almost disappear after 3000 psi-SCCO₂ treatment.

These results conform to the tendency in current-voltage characteristics and again verify that the SCCO₂ technology could effectively deactivate defects in HfO₂ films.

Another interesting detection, in Fig. 3-5, is the change of flat-band voltage of different-treated HfO₂ films under forward swing, also shown in table 3-1. For baking- treated HfO₂ film, the flat-band voltage (= -3.2 volt.) is away from ideal gate bias voltage (about 0~0.3 volt.), and that of 3000 psi-SCCO₂ treated HfO₂ is zeroed nearly. The main reason could be referred to (1) the positively charged Hf dangling bonds are passivated, (2) the fixed positive charges are removed by SCCO₂ fluids. The mechanism of extracting of fixed charge is shown in Fig. 3-6, including positive and negative fixed charge [57]. The polarized-H₂O molecule is taken as a dipole which would attract the fixed charge in HfO₂ films. Afterward, the H₂O molecule and fixed charge are carried away by SCCO₂ fluids mixed with propyl alcohol. For H₂O

vapor-treated HfO₂ film, the un-zeroed flat-band voltage could be attributed to (1) partial positively charged Hf dangling bonds remain, (2) the poorer capability for H₂O vapor to remove fixed charge. Hence, it is necessary for H₂O molecule to be driven into HfO₂ films and carried away by SCCO₂ fluids.

As a matter of fact, upon reducing the oxide thickness, it is difficult to calculate the density of interface states by using the high-low frequency method because of the substantially increased gate leakage current. Therefore, the interface capacitance (C_{it}) was employed instead of interface states to investigate the interfacial property.

Figure 3-7 (a) and (b) illustrates the equivalent capacitance models of MOS structure without and with C_{it} , respectively [56]. For higher measuring frequency, fewer interface states could respond to the ac switching signal, so suiting to the model in Fig. 3-7 (a) and presenting lower measured capacitance. For lower measuring frequency, more interface states could respond to the ac switching signal, so suiting to the model in Fig. 3-7 (b) and presenting higher measured capacitance. Therefore, the separation of C_{max} under different measuring frequency appears if the interface states existing. Figure 3-8 shows the capacitance-voltage characteristics of HfO₂ films after different treatment, measuring at 1M Hz and 100k Hz with forward gate bias swing. A conspicuous separation occurs in baking-treated HfO₂ films, and the higher density of interface states is supposed. However, with 3000 psi-SCCO₂ treatment, the value of C_{max} has only very slight rise under different measuring frequency, proofing that the effectively reducing interface states during SCCO₂ process. The sharp slope in transient region of C-V curve thereby is also reasonable.

3.1.4 Breakdown voltage measurement and gate bias stress

Figure 3-9 (a) and (b) show the breakdown characteristic curves of HfO₂ films after various treatments at positive and negative gate bias region, individually. The

breakdown voltage is mainly relative to the qualities of dielectric films and the density of defects in the dielectric films. A large number of traps lead to the trap-assisted tunneling early occurs and a high leakage current appears at small electric field, such that the lower breakdown voltages of dielectric films comes up. In Fig. 3-10 (a) and (b), whether at negative or positive gate bias, the baking-treated HfO_2 film presents the worst performance in breakdown voltage because of the high density of defects, and the improvements of breakdown voltage are gradually achieved via H_2O vapor and 3000 psi- SCCO_2 treatment. This result exhibits clearly that the density of defects in HfO_2 films are effectively reduced, and the breakdown voltage of 7nm HfO_2 film thereby could be substantially ameliorated from 1 V to 24 V at negative gate bias, from 30 V to 55 V at positive gate bias. It also indicates that the SCCO_2 fluids technology is greatly useful to enhance the low-temperature deposited HfO_2 films by passivating defects, and allows the treated HfO_2 film holding good reliability as the gate dielectric.

Another important property of dielectric films is the reliability under gate bias stress. Due to the gate dielectric is stressed at a high field when the transistors are operating, so that it is demanded for gate dielectric to have excellent resistance to the impairment under long time stress at operating electric field. During high electric field stress, the carriers of leakage current and high electric field would impact the weak bonding, leading to more defects, higher leakage current and the degradation of transistor [58]. Therefore, the reliability of dielectric under gate bias stress would judge whether agrees with the application of gate dielectric. Figure 3-10 shows the variation of leakage current of different-treated HfO_2 films as a function of stress time at a high electric field = 5 MV/cm, where I_0 is the initial leakage density. As well as the tendency of the measurement of breakdown voltage, the baking-treated HfO_2 film

behaves the most rises in the degree of leakage current as the stress time increasing, because of the great amount of defects and weak bonding. However, after treating with 3000 psi-SCCO₂ process, the sputter-deposited HfO₂ film performs a fine reliability under high electric field stress, hence it is extremely suitable for the application of gate dielectric.

3.2 Thin Film Analysis of Material and Discussion

3.2.1 Fourier Trans-form Infrared Spectroscopy (FTIR) Analysis

Fig. 3-11 shows the FTIR spectra of HfO₂ films after various post-treatments, including Baking-only, H₂O vapor and 3000 psi-SCCO₂ treatment. The functional group referred to Hf-O-Hf bonding is at 509 cm⁻¹ and 690 cm⁻¹, and the absorption peak at around 1070 cm⁻¹ attributes to the Si-O-Si bond. The Si-O-Si bond originates from the formation of interface layer (SiO_x) between HfO₂ film and silicon wafer during fabricating HfO₂ films in Ar/O₂ ambient. The peak intensity of Si-O-Si bond for different treatments is almost the same, meaning that these post-treatments would not make different influence on the thickness and quality of the interfacial SiO_x film. For the H₂O-vapor-treated HfO₂ film, however, the peak intensity of Hf-O-Hf bands (509 cm⁻¹ and 690 cm⁻¹) raises apparently in comparison with the baking-only-treated HfO₂ film. This is believed well that the H₂O vapor would permeate into HfO₂ film and makes reaction with Hf dangling bonds (i.e. traps) forming Hf-O-Hf bands. These traps in the low-temperature deposited HfO₂ film could be thereby passivated by H₂O vapor molecules. Furthermore, with 3000 psi- SCCO₂ treatment, obvious increase in the intensity of Hf-O-Hf bonding is observed in the FTIR. It indicates that the best transport efficiency of H₂O molecules into HfO₂ film is achieved by the SCCO₂ fluids, potentially modifying the dielectric properties of HfO₂ film, and the transporting

mechanism for SCCO₂ fluids taking H₂O molecule into HfO₂ film is shown in Fig. 3-12.

3.2.2 Thermal Desorption System – Atmospheric Pressure Ionization Mass Spectrometer (TDS-APIMS) Analysis

The TDS measurement, as shown in the Fig. 3-13, was carried out upon heating these treated HfO₂ films from 50 to 800 °C at a heating rate of 10 °C/min in vacuum (10⁻⁵ Pa.). In Fig. 3-13 (a), m/e (mass-to-charge ratio) = 32 peak that is attributed to O₂ was monitored to evaluate the content of oxygen outgassing from HfO₂ films. It is clearly found the highest oxygen content is detected in the 3000 psi-SCCO₂ treated HfO₂ film, certainly consistent with the FTIR observation. From Fig. 3-13 (b), m/e (mass-to-charge ratio) = 44 peak that is attributed to CO₂, the residual carbon dioxide in HfO₂ is equal after various post-treatments. This is result from SCCO₂ fluid not only employed to transport the CO₂ molecule into HfO₂ film but the CO₂ molecule is not remain in addition [21, 22].

3.2.3 X-ray Photoelectron Spectroscopy (XPS) Analysis

XPS involves measuring the photoelectron spectra obtained when a sample surface is irradiated with x-rays. The kinetic energy (peak position) of the photoelectrons can be written as

$$E_K = h\nu - E_B - \phi_s - q\phi \quad (3.12)$$

where $h\nu$ is the x-ray energy, E_B is the binding energy (the difference between the Fermi level and the energy level being measured), ϕ_s is the work function of the electron spectrometer, q is the electronic charge, and ϕ is the surface potential.

We have also performed XPS measurements using an Al K α X-ray source (1486.6 eV photons) to determine the bonding environments of the Hf and O atoms.

Figure 3-14 shows the O 1s core level peaks also demonstrated binding energy shift with changing of different post-treatments. Each peak can be split into two sub-peaks by Gaussian fitting which represent the Hf-O bonding at ~530.1 eV and O-Si bonding at ~531.5 eV [59,60]. The peak intensity of O-Si bond for different treatments is almost the same, meaning that these post-treatments would not make different influence on the thickness and quality of the interfacial SiO_x film. For the H₂O-vapor-treated HfO₂ film, however, the peak intensity of Hf-O bands raises apparently in comparison with the baking-only-treated HfO₂ film. This is believed well that the H₂O vapor would permeate into HfO₂ film and makes reaction with Hf dangling bonds (i.e. traps) forming Hf-O bands. These traps in the low-temperature deposited HfO₂ film could be thereby passivated by H₂O vapor molecules. Furthermore, with SCCO₂ treatment, obvious increase in the intensity of Hf-O bonding is observed in the XPS. It indicates that the best transport efficiency of H₂O molecules into HfO₂ film is achieved by the SCCO₂ fluids, potentially modifying the dielectric properties of HfO₂ film, and the transporting mechanism for SCCO₂ fluids taking H₂O molecule into HfO₂ film is shown in Fig. 3-12.

3.2.4 Transmission Electron Microscopy (TEM) Analysis

Figure 3-15 (a), (b), (c) show the influence of various post-treatments on HfO₂ thin film samples in TEM material analysis. The first group labeled as Baking-only treatment, was designed as the control sample, and was only baked on a hot plate at 150 °C for 2 hrs. The second group labeled as H₂O vapor treatment, was immersed into a pure H₂O vapor ambience at 150 °C for 2 hrs in a pressure-proof stainless steel chamber with a volume of 100cm³. The third group marked as 3000psi-SCCO₂ treatment, was placed in the supercritical fluid system at 150°C for 2 hrs, where was

injected with 3000psi of SCCO₂ fluids mixed with 5 vol.% of propyl alcohol and 5 vol.% of pure H₂O. The interfacial layer of SiO_x for different treatments is almost the same. It is found that 3000psi-SCCO₂ treatment can improve performance of MIS, including leakage current density suppression and EOT reduction. On the other hand, the k value of Baking-only-treated, H₂O-vapor-treated and 3000psi-SCCO₂-treated HfO₂ film is about 20.4, 24.8 and 29.4. The k value is increased and interfacial layer is almost the same. It can be understood reasonably that during 3000psi-SCCO₂-treated HfO₂ film is dense and thickness of interfacial layer is increasing a little due to oxygen penetration. The detail discussion would be in 3.1.3.

3.3 OTFTs Analysis of Electrical Characteristics and Discussion

3.3.1 The current density-electric field (J - E) characteristics

The leakage current densities of HfO₂ films after different treatments are shown as a function of applied negative gate bias voltage to positive gate bias voltage in Fig. 3-16. Among various post-treatments, the baking-treated HfO₂ film exhibits the most serious leakage current, inferentially due to its poor dielectric characteristics with numerous traps inside the HfO₂ film and the interface between parasitical SiO_x and Si wafer. The improvement of electrical characteristics is observed by using H₂O vapor process, however, a high leakage current density still appears at larger applied voltages. It could be inferred reasonably dependent on the defect passivation efficiency. The most indicating that H₂O vapor can passivate the traps (or defects) and alter dielectric properties of the low-temperature-deposited HfO₂ film. After H₂O vapor treatment, effective improvement of electrical characteristic is obtained by the 3000 psi-SCCO₂ treatment, exhibiting the lowest leakage current density among all samples. Low leakage current density ($\sim 2 \times 10^{-6}$ A/cm²) is kept constantly, even biased

at an electric field of 1.33 MV/cm.

3.3.2 The capacitance-voltage (*C-V*) characteristics

The capacitance-voltage (*C-V*) characteristics are also generally used to judge the quality of dielectric films. Figure 3-17 shows capacitance-voltage characteristics of HfO₂ films after different treatment, measuring at 1M Hz with gate bias swing from negative voltage to positive voltage (forward) and from positive voltage to negative voltage (reverse). The slope of *C-V* curve in transient region, i.e. from C_{\max} to C_{\min} , is relative to the interface states, for example, the sharp slope indicates fewer defects exist in the interface between HfO₂ and Si wafer. In Fig. 3-17, the baking-treated HfO₂ film presents the worst *C-V* curve and lower capacitance. This expresses the larger number of interface states exist and lead to the smooth *C-V* curve. With H₂O vapor treatment, the sharper *C-V* curve and higher capacitance are obtained, and it could be attributed to the reduction of defects in HfO₂ film and the interface. Furthermore, the best improvement is achieved by 3000 psi-SCCO₂ treatment. This exhibits that the SCCO₂ treatment possesses excellent ability to passivate the defects, including Hf dangling bonds and interface states.

Besides, from Fig. 3-17, the shift of *C-V* curve under forward and reverse swing is also appears in baking-treated and H₂O vapor-treated HfO₂ films. It is resulted from the trapped carrier in defects of HfO₂ films, and that is not expected for gate insulator of transistors. Under negative gate bias, the electric inject from Al gate into HfO₂ films and trapped by defects, leading to the larger gate bias is required for inducing electron-inversion layer. It is evidently observed that the baking-treated HfO₂ film hold numerous defects because of the extensive shift of flat-band voltage, and the defects almost disappear after 3000 psi-SCCO₂ treatment.

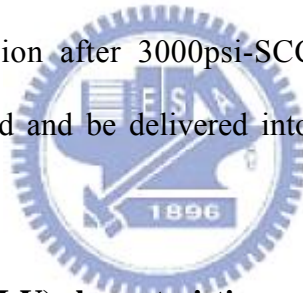
These results conform to the tendency in current-voltage characteristics and again verify that the SCCO₂ technology could effectively deactivate defects in HfO₂ films.

In another interesting detection, in Fig. 3-17. The baking- treated HfO₂ film, the flat-band voltage (= -0.3 volt.) is away from ideal gate bias voltage (about 0~0.3 volt.), and that of 3000 psi-SCCO₂ treated HfO₂ is zeroed nearly. The main reason could be referred to (1) the positively charged Hf dangling bonds are passivated, (2) the fixed positive charges are removed by SCCO₂ fluids. The mechanism of extracting of fixed charge is shown in Fig. 3-6, including positive and negative fixed charge [57]. The polarized-H₂O molecule is taken as a dipole which would attract the fixed charge in HfO₂ films. Afterward, the H₂O molecule and fixed charge are carried away by SCCO₂ fluids mixed with propyl alcohol. For H₂O vapor-treated HfO₂ film, the un-zeroed flat-band voltage could be attributed to (1) partial positively charged Hf dangling bonds remain, (2) the poorer capability for H₂O vapor to remove fixed charge. Hence, it is necessary for H₂O molecule to be driven into HfO₂ films and carried away by SCCO₂ fluids.

3.3.3 Secondary Ions Mass Spectrometer (SIMS) Analysis

The means of secondary ion mass spectroscopy (SIMS) analyzed by using various elements profiles in the dielectrics. During SIMS analysis [61], the surface of the sample is subjected to Cs⁺ ion bombardment with energy of 5.78 KeV and negative secondary ions. The bombarding primary ion beam (Cs⁺) produces monatomic and polyatomic particles of sample material and re-sputtered primary ions, along with electrons and photons. This leads to the ejection of both neutral and charged species from the surface. Monitoring the secondary ion count rate of the selected element as a function of time leads to depth profiles.

Fig. 3-18 (a), (b) and (c) show the SIMS profiles of the hafnium oxide film after various post-treatments, including Baking-only and 3000 psi-SCCO₂ treatment. The first group labeled as Baking-only treatment, was designed as the control sample, and was only baked on a hot plate at 150 °C for 2 hrs. The second group labeled as 3000psi-SCCO₂ treatment, was placed in the supercritical fluid system at 150°C for 2 hrs, where was injected with 3000psi of SCCO₂ fluids mixed with 5 vol.% of propyl alcohol and 5 vol.% of pure H₂O. In Fig. 3-17 (a) and (b), the baking-only-treated and 3000 psi-SCCO₂-treated films had the nearly same quantity of Silicon and Hafnium atoms. The expression after 3000psi-SCCO₂ treatment, Silicon and Hafnium atoms quantity had not evident increased. Hafnium atoms had few diffused to the Silicon substrate. In Fig. 3-17 (c), the 3000 psi-SCCO₂-treated films had more quantity Oxygen atoms. The expression after 3000psi-SCCO₂ treatment, Oxygen atoms quantity had evident increased and be delivered into the HfO₂ film for passivating defects.



3.3.4 The current-voltage (I-V) characteristics

In this series of experiment, we compare devices of HfO₂ film with different various post-treatments, including Baking-only, H₂O vapor and 3000 psi-SCCO₂ treatment and PECVD SiO₂ film is control group. The channel width is 800μm and length is 600μm. In Fig. 3-18 (a) and (b) for I_D-V_G characteristics, Using baking only and H₂O vapor treatment, the device are not accomplished. The gate current is almost the same as drain current. It indicates that the leakage current is still large after baking only and H₂O vapor treatment on HfO₂ gate dielectrics. In Fig. 3-19(a) and (b) for drain current-drain voltage (I_D-V_G) characteristics, the gate bias ranged from 10 to -20V, and the drain voltage -10V are provided for the device. We can also compare devices with different insulator. From the I_D-V_G chart, the turn-on current of 3000

psi-SCCO₂ treatment for HfO₂ insulator of OTFTs great than PECVD SiO₂ insulator for OTFTs. The turn-off current of 3000 psi-SCCO₂ treatment for HfO₂ insulator for OTFTs is lower than SiO₂ insulator for OTFTs. From the I_D - V_G data, we can extract the mobility and threshold voltage from the square-root of drain current versus gate voltage curves and extract the on/off current ratio from the ratio of maximum turn-on current versus minimum turn-off current. The mobility of $0.05\text{cm}^2/\text{V} \cdot \text{s}$ 、threshold voltage of -0.1V 、sub-threshold swing of 2.2 volt/dec and on/off current ratio of 2×10^5 . The PECVD SiO₂ insulator of OTFTs had mobility of $0.026\text{cm}^2/\text{V} \cdot \text{s}$ 、threshold voltage of 2.1V 、sub-threshold swing of 3.6 volt/dec and on/off current ratio of 10^4 . The 3000 psi-SCCO₂ treatment for HfO₂ insulator for OTFT has good performance. In Fig. 3-20 for I_D - V_D characteristics, we provide the drain voltage from 0 to -20V and change the gate voltage from 0 to -30V , step by -10V . The I_D - V_D curves show the turn-on operation of the device. We can observe that the turn-on current is largest in the 3000 psi-SCCO₂ treatment for HfO₂ insulator for OTFT. In Fig. 3-21 for normalized of I_D - V_D characteristics, we can observe the 3000 psi-SCCO₂ treatment for HfO₂ insulator for OTFT had higher turn-on current and better on/off current ratio.

3.3.5 The DC bias and current stress characteristics

Under DC bias and current stress, the gate bias stress measurements were performed in atmosphere and darkness on OTFT on 3000 psi-SCCO₂ treatment for HfO₂ insulator and PECVD SiO₂ insulator. The stress gate voltage was -20V . The stress drain voltage and current were 0V , -20V and -200nA . Fig. 3-22 show a series of transfer curves at $t = 0$ 、 50 、 100 、 500 and 1000 sec on OTFT of 3000 psi-SCCO₂ treatment for HfO₂ insulator, between which $V_D = 0\text{V}$, -20V , and $I_D = -200\text{nA}$ respectively. In Fig. 3-22 indicates the increase of stress time from 0 to 50 、 100 、 500

and 1000 sec, respectively. Fig. 3.23 plots show the mobility decay with different stress times. Fig. 3.24 plots show the threshold voltage shift tended toward more negative with different stress times. Fig. 3-25 show a series of transfer curves at $t = 0, 50, 100, 500$ and 1000 sec on OTFT of PECVD SiO_2 insulator, between which $V_D = 0 \text{ V}$, -20V , and $I_D = -200\text{nA}$ respectively. In Fig. 3-25 indicates the increase of stress time from 0 to 50, 100, 500 and 1000 sec, respectively. Fig. 3-26 plots show the mobility decay with different stress times. Fig. 3-27 plots show the threshold voltage shift tended toward more negative with different stress times. The negative threshold voltage shift due to the negative gate bias stress may be attributed to the decrease of mobile holes in the channel via the charge trapping in the insulator. The two reasons would likely be concerned about negative threshold voltage shift. First, the dangling bonds in grain boundary would be considered for the reason of the mixed phase in thin film. The accumulated carriers hopping in channel through π bond facilitate charge trapping in the dangling bonds after a long operational period. Second, due to molecular extending structure in electrical filed, π bonds happened to out of control so that the hopping behavior was temporally abnormal and the less mobile states formed. If the stress is operated for the long time, the defect sites are more likely to form and trapping charges appear. The OTFT of PECVD SiO_2 insulator has good performance on threshold voltage shift and mobility decay because the SiO_2 has higher barrier than HfO_2 . The Stress is not serious for a long time.

3.4 Summary

We have demonstrated experimentally the effects of low-temperature treatments on the dielectric characteristics of HfO_2 film. The preliminary improvement in HfO_2 dielectrics is obtained by H_2O vapor immersion at 150°C , due to the deactivation of defects inside low-temperature deposited HfO_2 films and replacing these defects by the formation of Hf-O-Hf bonds. A further study also showed that the efficiency of passivating defects can be maximized via the SCCO_2 treatment which mixed with H_2O and additive alcohol. Basing on the gas-like and high-pressure properties, the supercritical CO_2 fluids can affinity with H_2O molecules and infiltrate into HfO_2 films to effectively deactivate these defects (or dangling bonds). After SCCO_2 treatment, the amount of oxygen and the intensity of Hf-O-Hf bonds obviously rise, and the superior resistance to leakage current is gained as a result of the conduction mechanism transform into Schottky emission. The properties of SCCO_2 -treated HfO_2 film, such as larger dielectric constant, lower density of interface states, higher breakdown voltage of HfO_2 film and excellent reliability under high electric field are presented in addition. These results indicate that the low-temperature SCCO_2 fluids technology is greatly beneficial to enhance the dielectric properties of low-temperature deposited HfO_2 films by reducing defects, and performs better electrical reliability. We have successful fabrication OTFTs with low-temperature treatments on the dielectric characteristics of HfO_2 insulator after. The characteristic of mobility, threshold voltage and on/off current ratio have better OTFT of PECVD SiO_2 insulator. The DC bias and current stress characteristics decay is nearly.

Chapter 4

Conclusion

In this study, we successfully employ the supercritical CO₂ fluids technology to carry H₂O molecule into sputter-deposited HfO₂ film for passivating the defects at low temperature and successfully obtained characteristics of OTFTs. The mobility of 0.05 cm²/Vs, threshold voltage of -0.1 V, on/off current ratio of 2×10⁵ and sub-threshold swing of 2.2 V/Dec. .

With this proposed treatment, the HfO₂ films present the more completed higher oxygen content and Hf-O-Hf binding. In the investigation on the electrical characteristics of treated-HfO₂ films, the excellent performances of dielectric property are achieved, including the ultra-low leakage current, the ideal capacitance-voltage curve, the higher dielectric constant, the better resistance to breakdown and the more stable reliability under high electric field. From these experimental results, the efficiency of applying supercritical CO₂ fluids to deactivate defects is proved. Therefore, this technology agrees to fabricate the high quality dielectric films at low-temperature.

This proposed technology is also used to fabrication organic thin film transistors (OTFTs) at 150 °C. After supercritical CO₂ treatment, we successfully obtained characteristics of OTFTs are better than SiO₂ insulator of OTFTs, including the better sub-threshold swing, lower off-current, higher on/off current ratio and higher mobility. The DC bias and current stress characteristics were nearly SiO₂ insulator of OTFTs. Such that the supercritical CO₂ treatment provide a novel method to fabricated OTFTs at low-temperature.

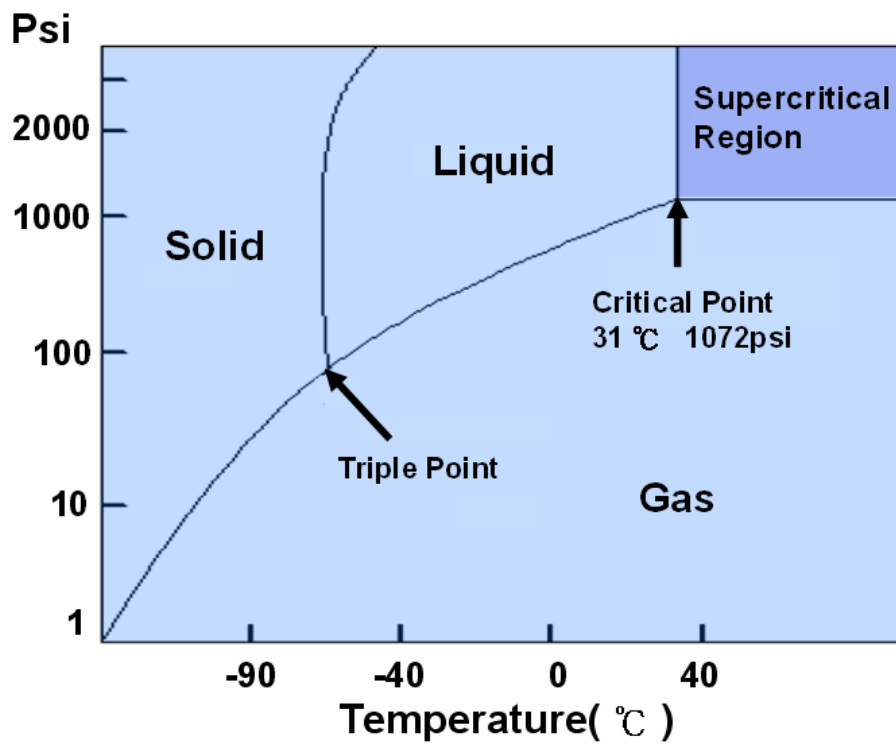


Fig. 1-1 Phase diagram for CO₂.

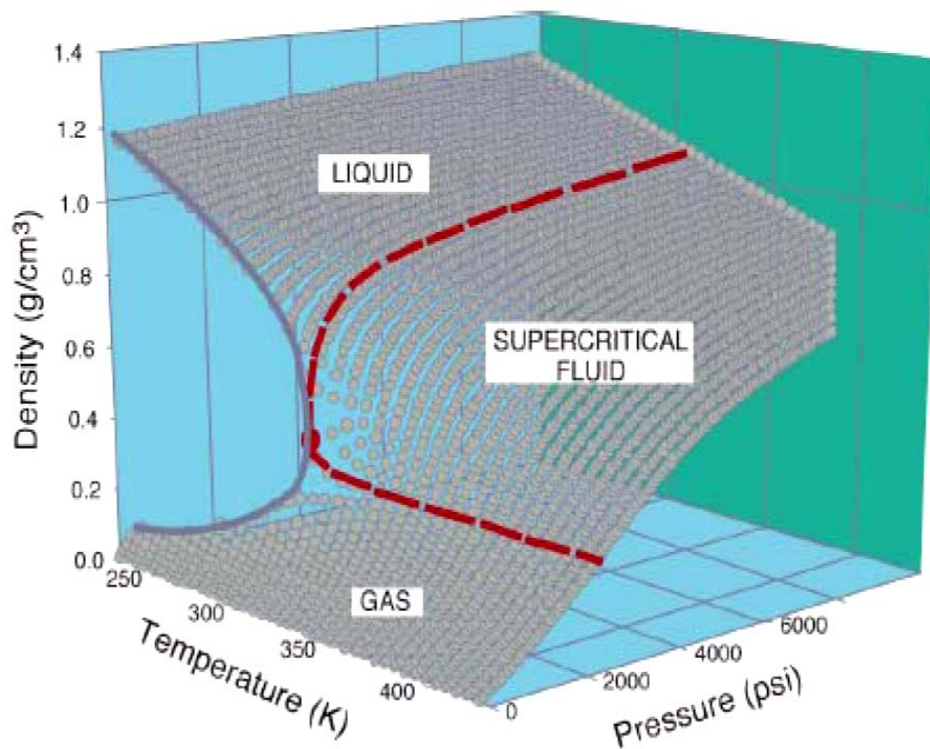



Fig. 1-2 Density-pressure-temperature surface for pure CO₂.

Fluid	Critical Temperature(°C)	Critical Pressure (Psi) (1atm=14.7psi)
Helium (He)	-268	33
Neon (Ne)	-229	400
Argon (Ar)	-122	706
Nitrogen (N ₂)	-147	492
Oxygen (O ₂)	-119	731
Carbon dioxide (CO ₂)	31	1072
Sulfur hexafluoride (SF ₆)	46	545
Ammonia (NH ₃)	133	1654
Water (H ₂ O)	374	3209

Table 1-1 Critical temperature and pressure for some common fluids.



	Liquid	Supercritical Fluid	Vapor
Density (g/cm ³)	1.0	0.3 ~ 0.7	~ 10 ⁻³
Diffusivity (cm ² /sec)	< 10 ⁻⁵	10 ⁻² ~ 10 ⁻⁵	~ 10 ⁻¹
Viscosity (g/cm-sec)	~ 10 ⁻²	10 ⁻³ ~ 10 ⁻⁶	~ 10 ⁻⁶

Table 1-2 Comparison of physical properties of CO₂.

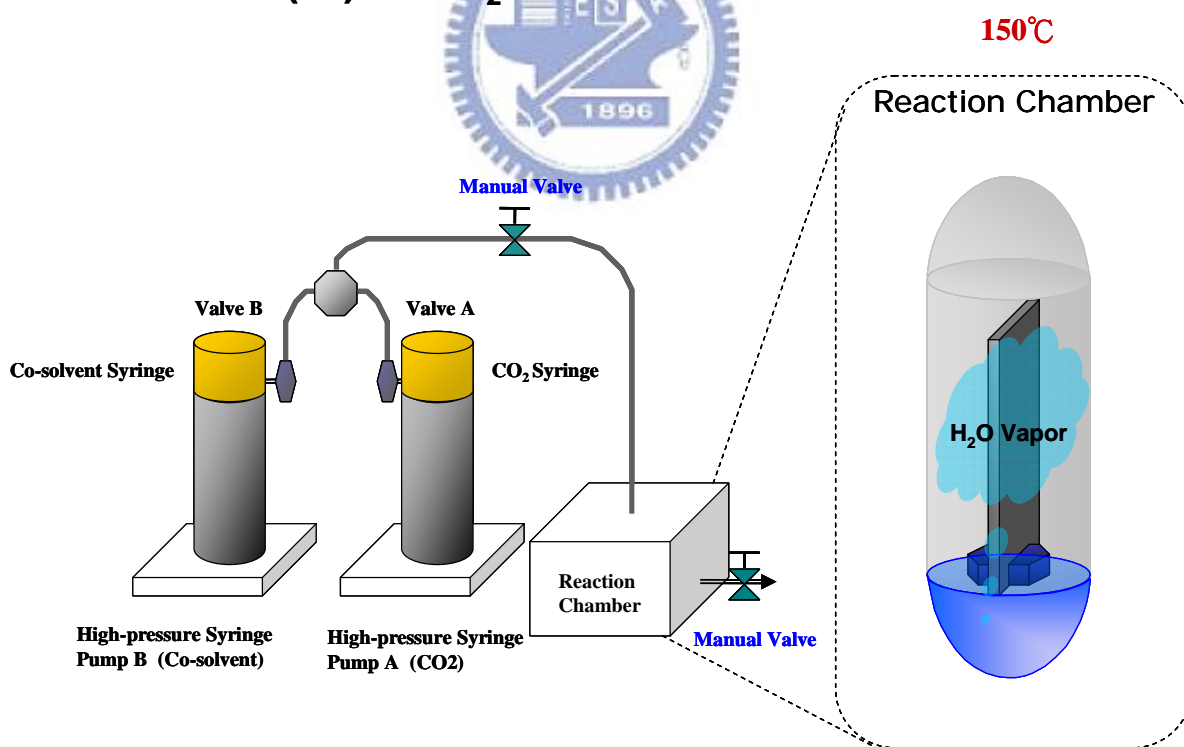
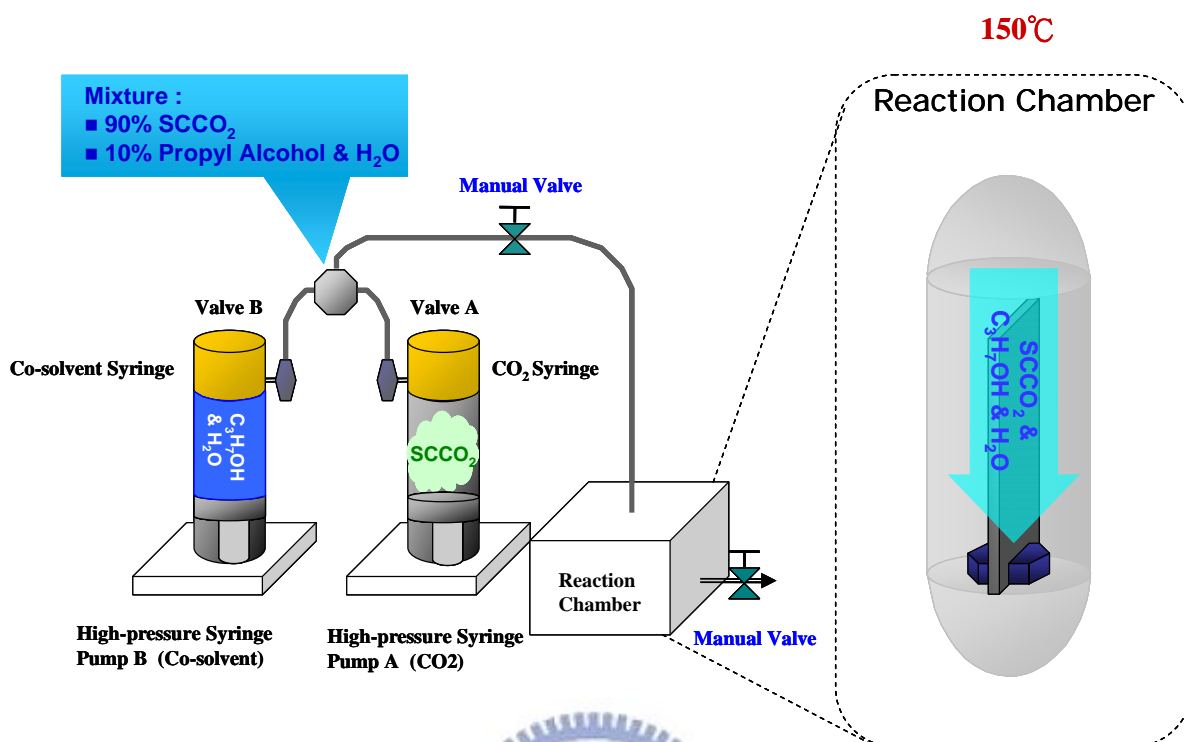
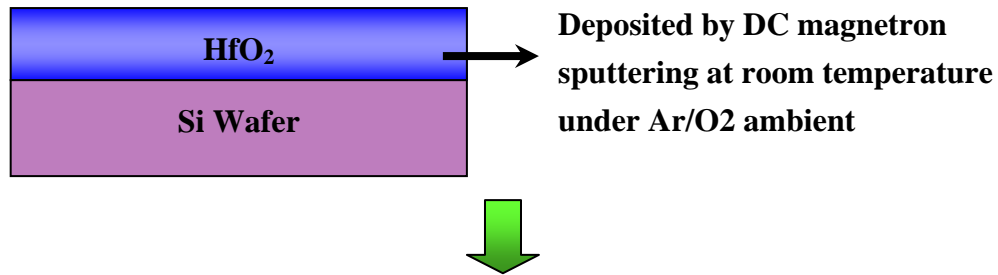


Fig. 2-1 The supercritical fluid system.

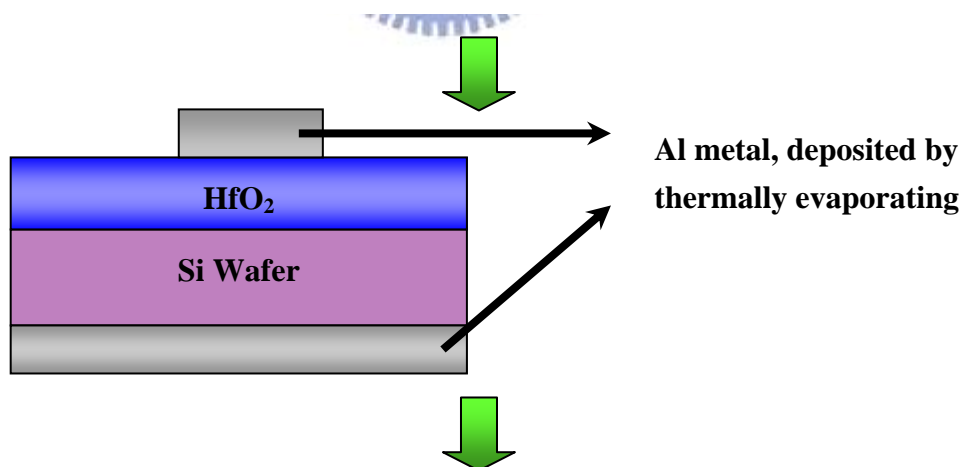


Defect passivation process:

1. **Baking-only treatment :**
only baked on a hot plate at 150 °C for 2 hrs.
2. **H₂O vapor treatment :**
immersed into a pure H₂O vapor ambience at 150 °C for 2 hrs.
3. **3000psi-SCCO₂ treatment :**
was placed in the supercritical fluid system at 150°C for 2 hrs.



1. **Fourier transformation infrared spectroscopy (FTIR).**
2. **Thermal desorption spectroscopy (TDS).**
3. **X-ray Photoelectron Spectroscopy (XPS).**
4. **Transmission Electron Microscopy (TEM).**



1. **Current density-electric field (J-E) characteristics.**
2. **Capacitor-voltage (C-V) characteristics.**
3. **Breakdown voltage**
4. **Gate bias stress**

Fig. 2-2 The experiment processes of thin HfO₂ film with various treatments.

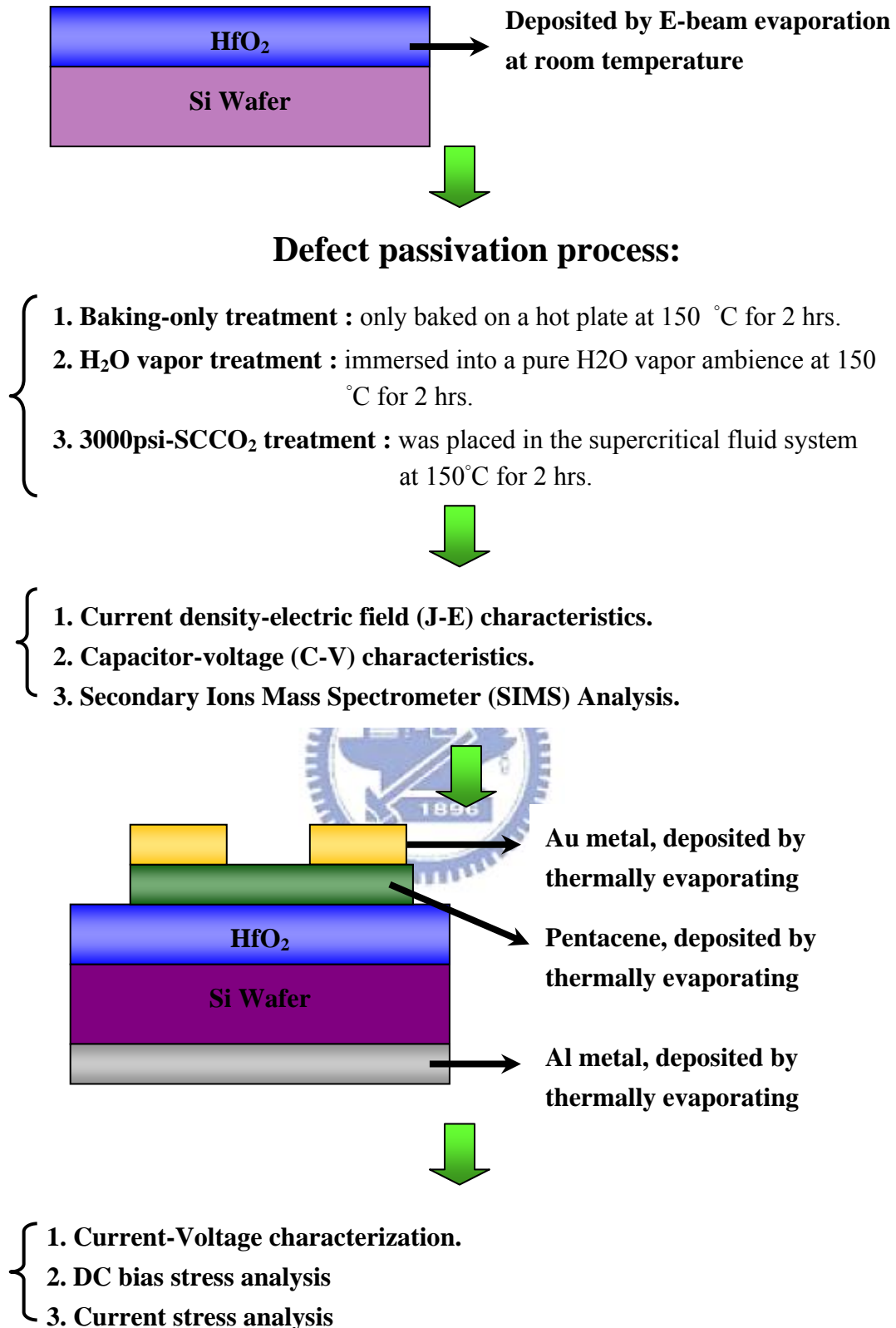


Fig. 2-3 The experiment processes of OTFTs with HfO₂ film of various treatments .

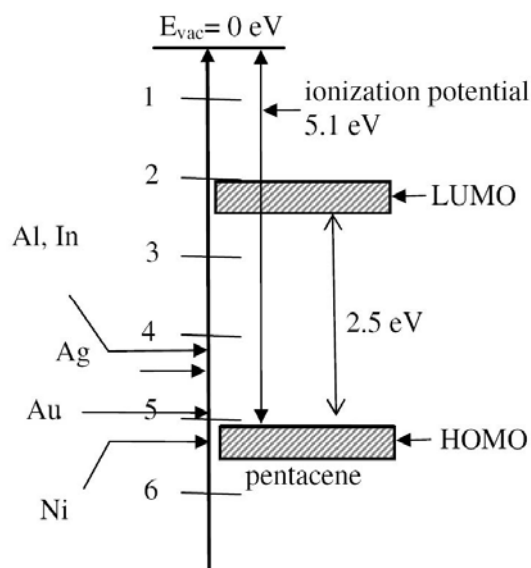


Fig. 2-4 The energy band diagram of pentacene. The optical energy gap and adiabatic energy gap are determined.

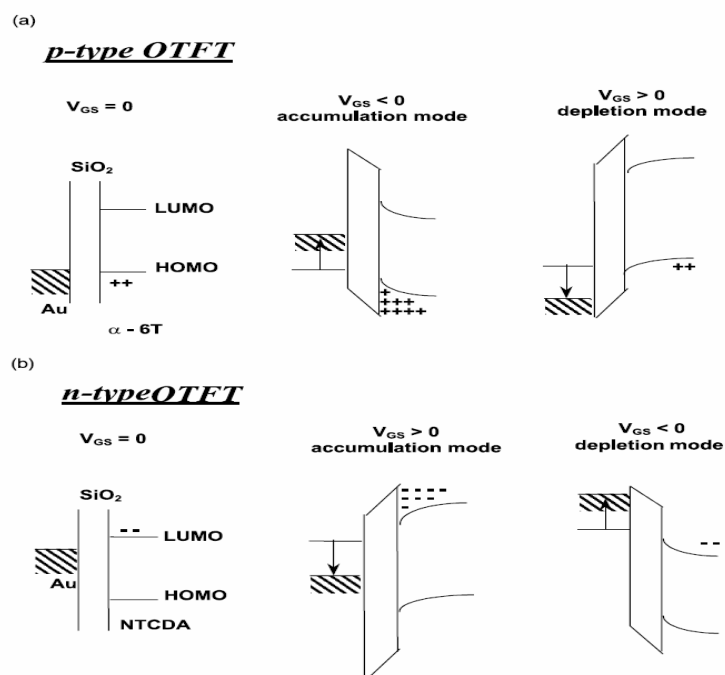


Fig. 2-5 Energy band diagrams (a) for a p-channel (pentacene) and (b) for a n-channel (NTCDA) OTFTs. The left side shows the devices at zero gate bias, while in the centre and in the right parts the accumulation and depletion mode operation regimes are presented.

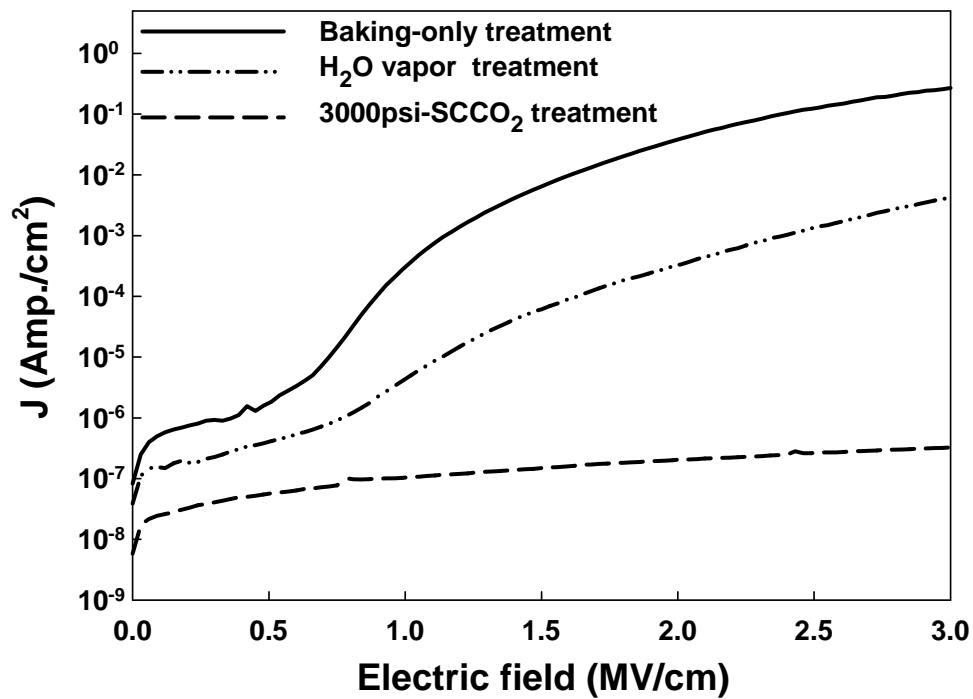


Fig. 3-1 The leakage current densities of HfO₂ films after different treatments (The negative bias is applied on gate electrode)

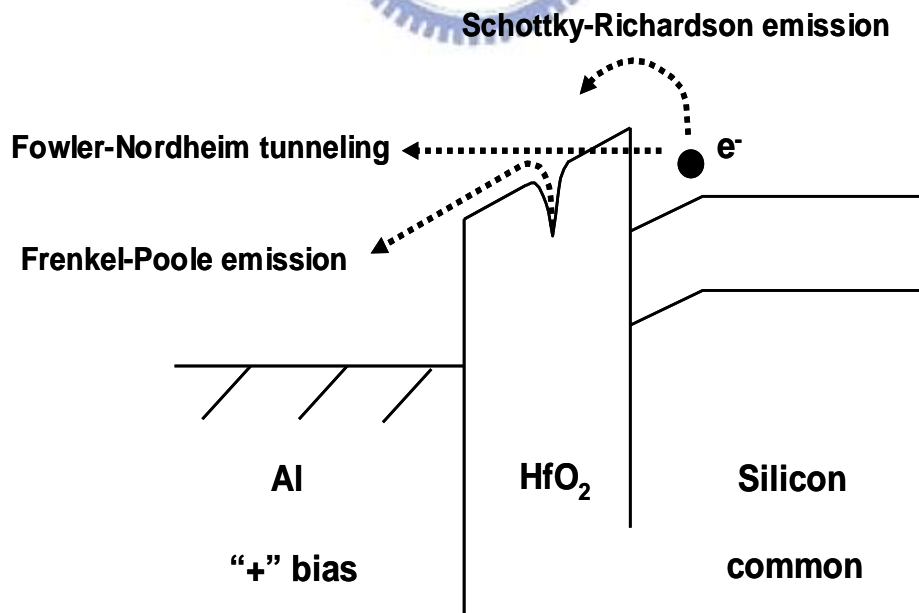


Fig. 3-2 Conduction mechanism for Al/HfO₂/Si MIS structure.

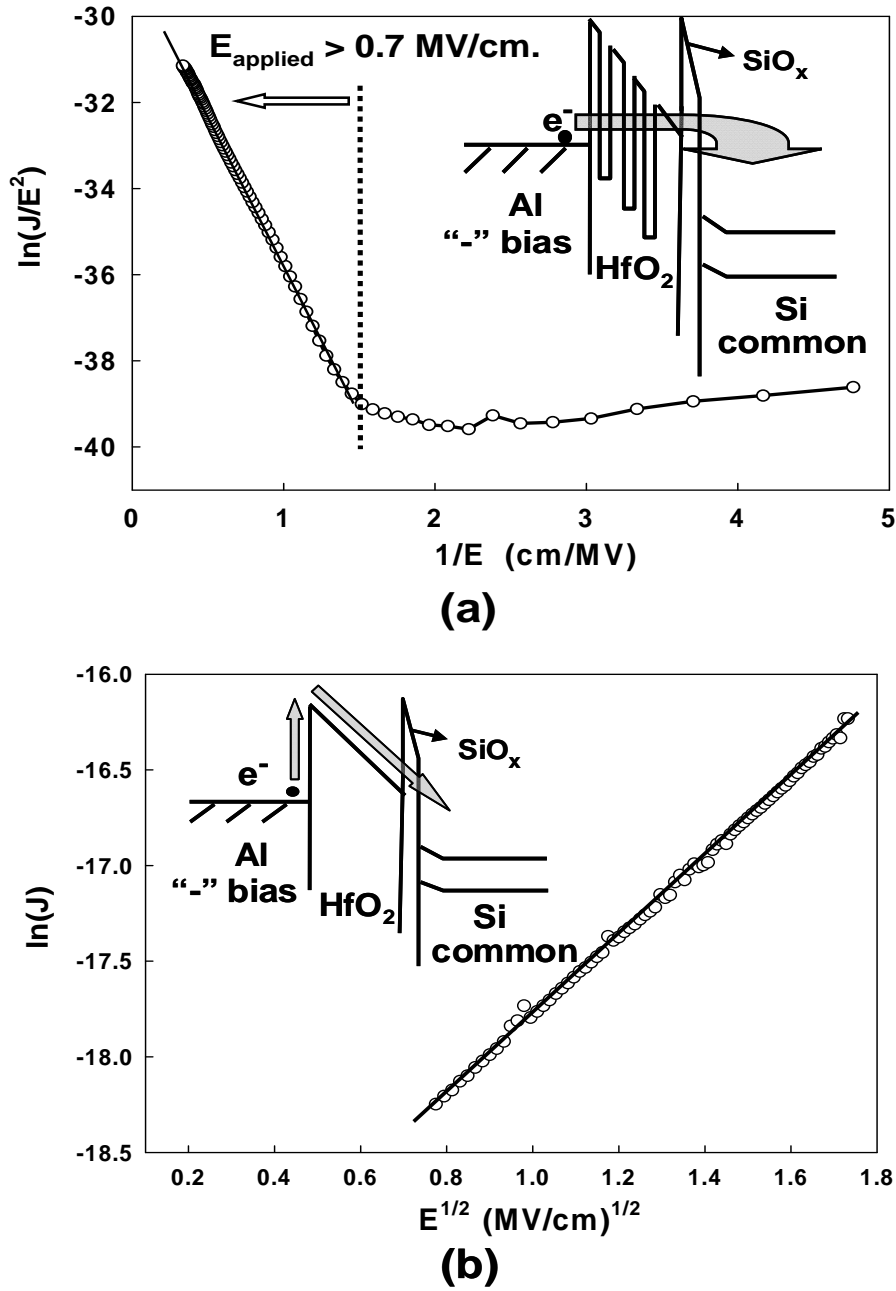


Fig. 3-3 (a) Curve of $\ln(J/E)$ versus reciprocal of electric field ($1/E$) for the baking-only treated HfO₂ film, and a schematic energy band diagram accounting for trap-assisted tunneling shown in the inset. (b) Leakage current density versus the square root of electric field ($E^{1/2}$) plot for the 3000 psi-SCCO₂ treated HfO₂ film. The inset shows the energy band diagram of Schottky-type conduction mechanism.

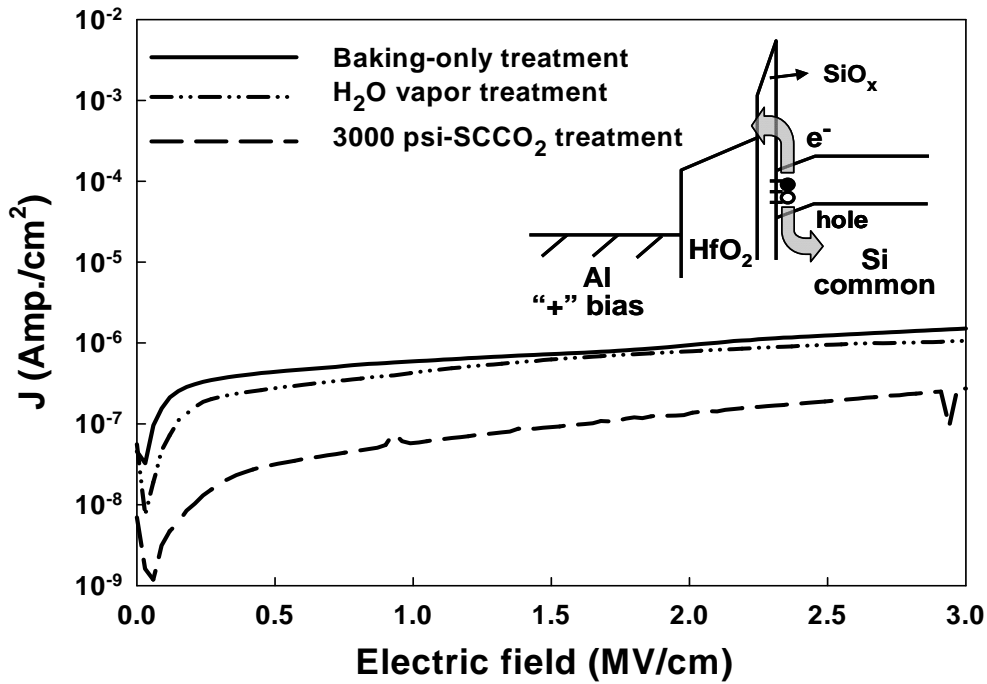


Fig. 3-4 The leakage current densities of HfO₂ films after different treatments (The positive bias is applied on gate electrode).

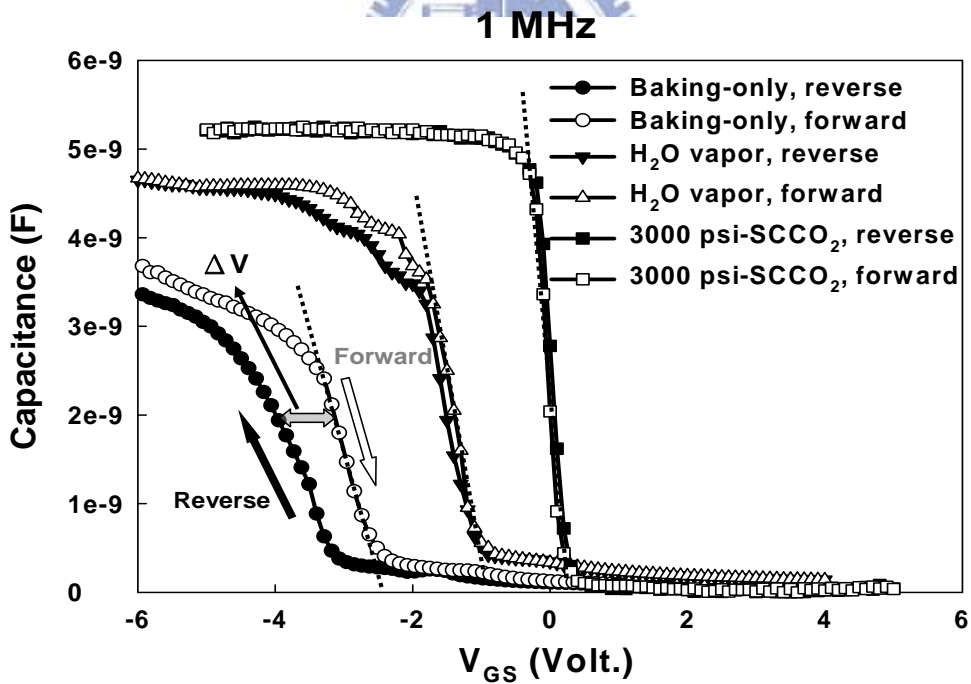


Fig. 3-5 The capacitance-voltage characteristics of HfO₂ films after different treatment, measuring at 1M Hz with gate bias swing from negative voltage to positive voltage (forward) and from positive voltage to negative voltage (reverse)

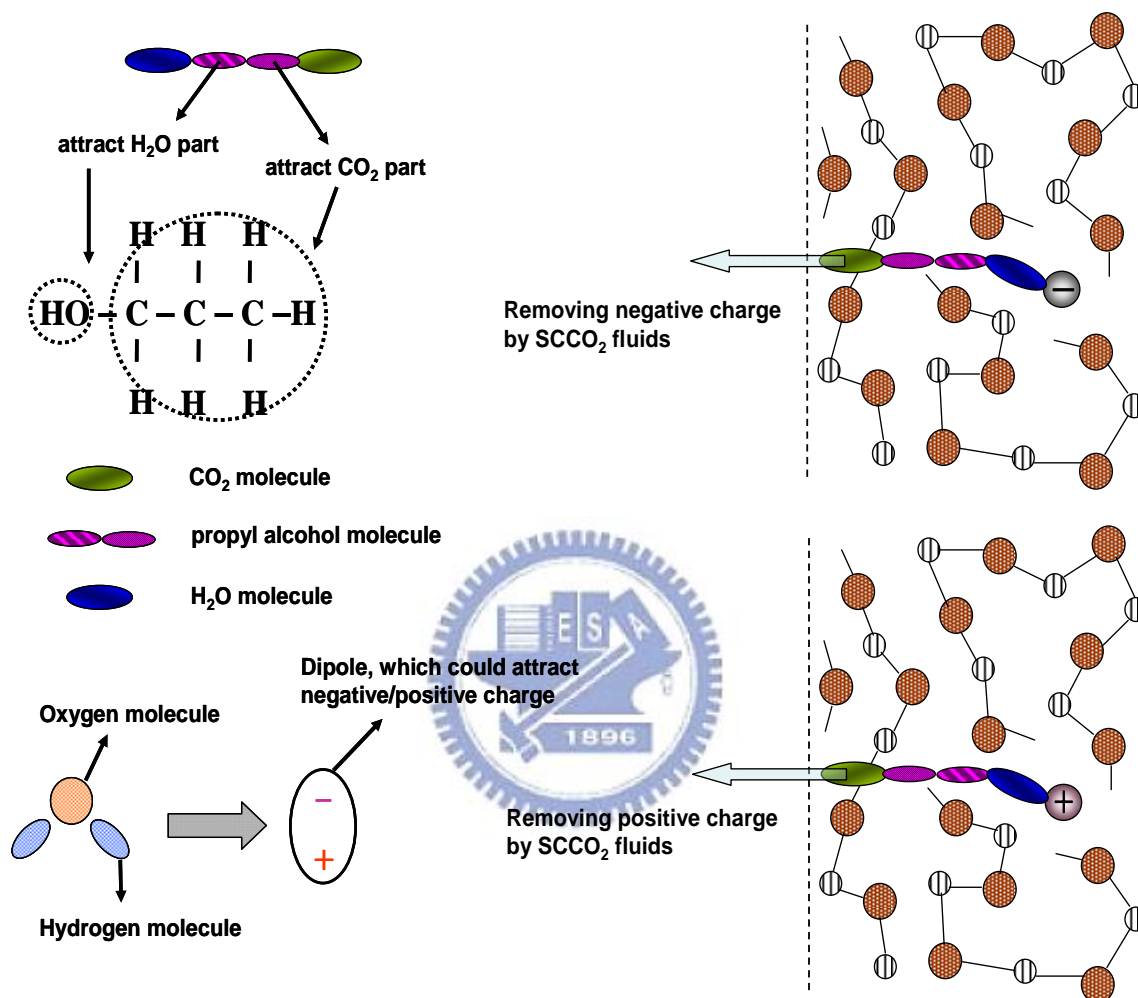


Fig. 3-6 The mechanism of extracting of fixed charge with SCCO₂ fluids.

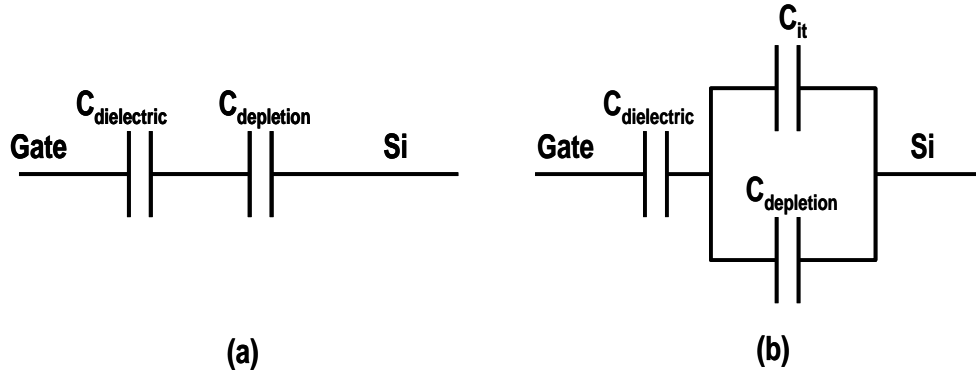


Fig. 3-7 The equivalent capacitance models of MOS structure (a) without C_{it} , (b) with C_{it} .

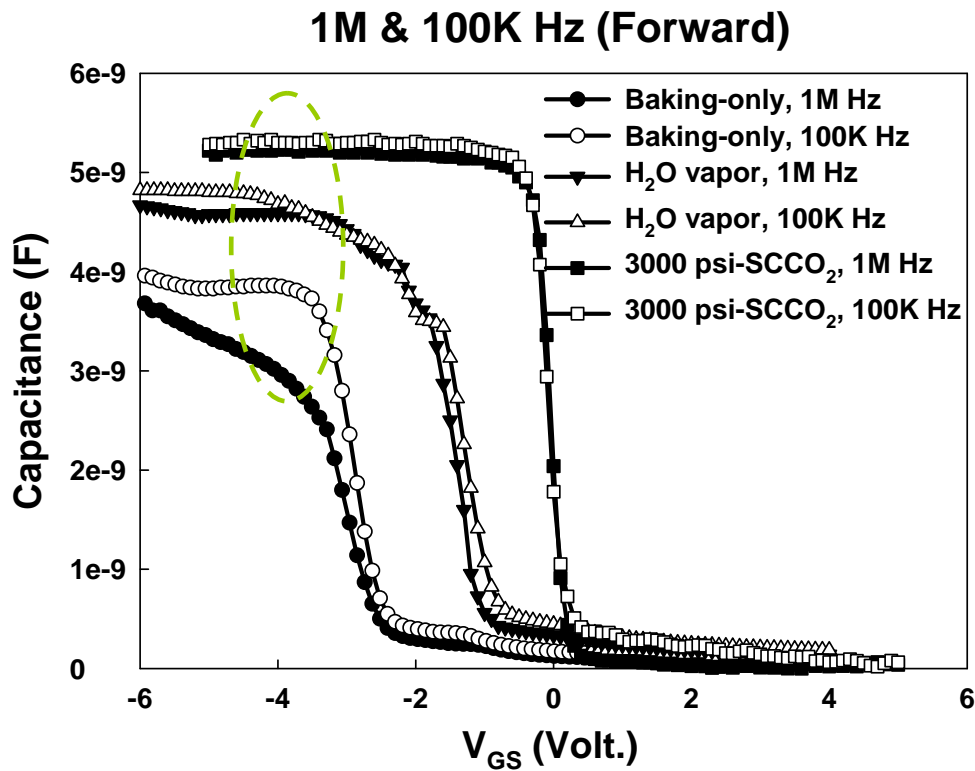


Fig. 3-8 The capacitance-voltage characteristics of HfO_2 films after different treatment, measuring at 1M Hz and 100k Hz with forward gate bias swing.

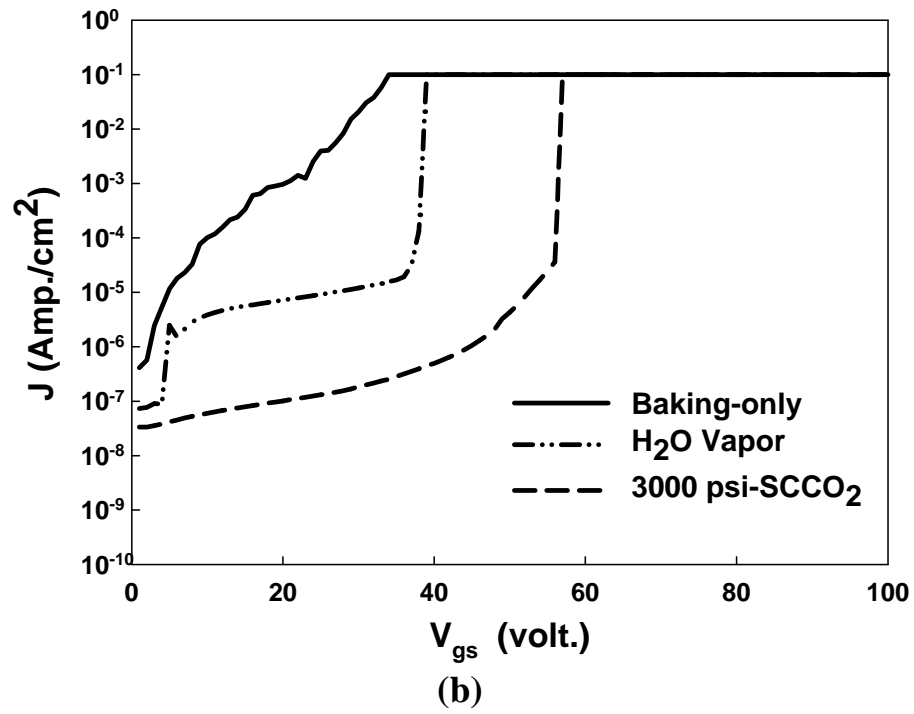
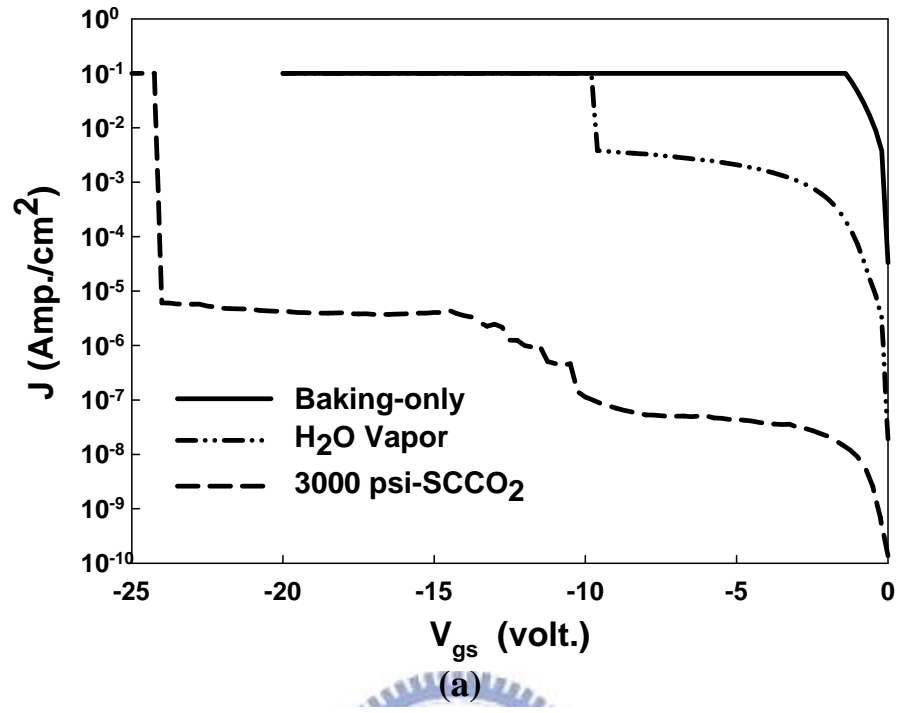


Fig. 3-9 The breakdown characteristic curves of HfO₂ films after various treatments (a) at positive and (b) at negative gate bias region, individually.

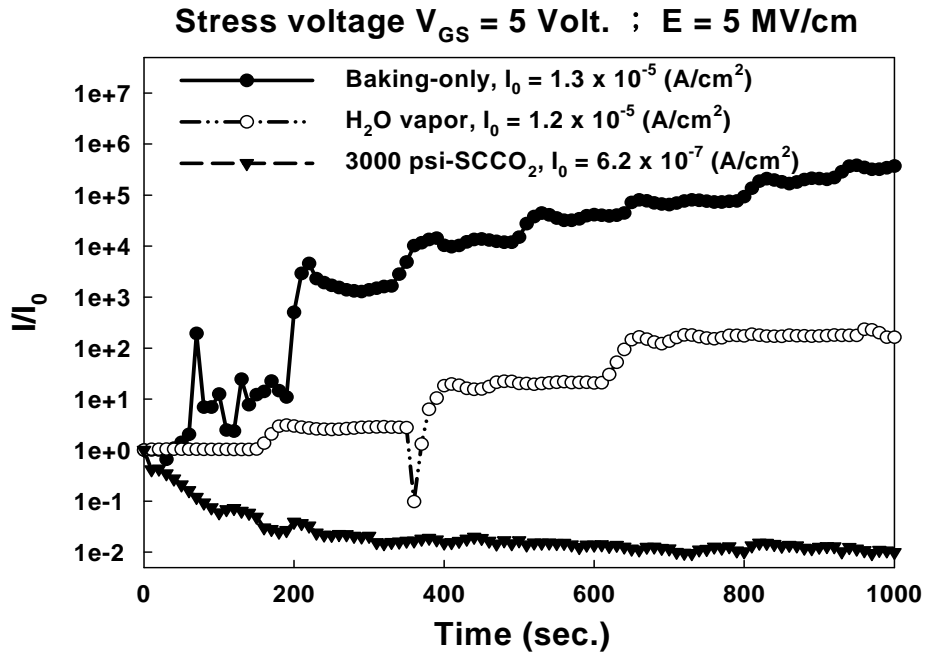


Fig. 3-10 The variation of leakage current of different-treated HfO_2 films as a function of stress time at a high electric field = 5 MV/cm.

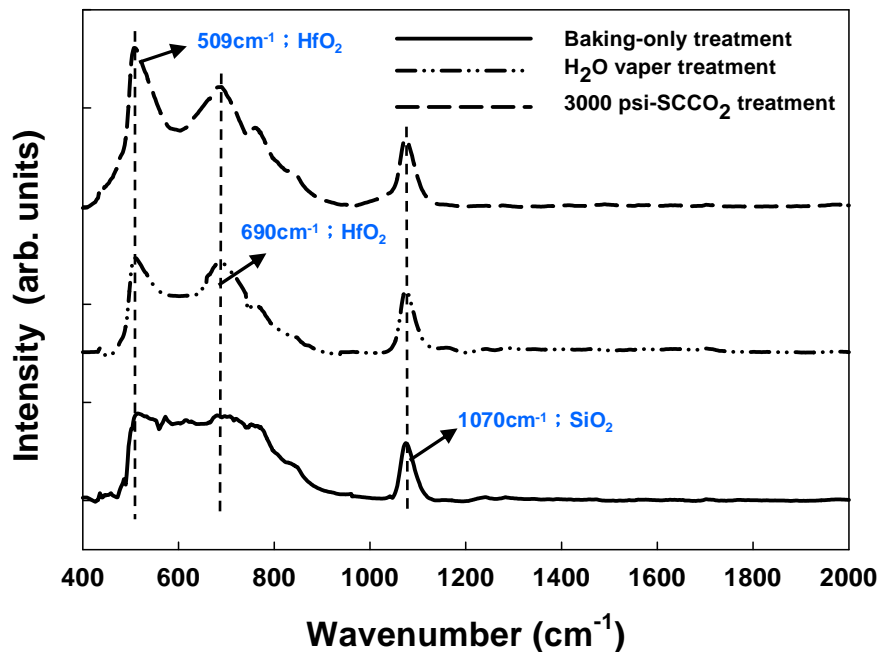


Fig. 3-11 The FTIR spectra of HfO_2 films after various post-treatments, including Baking-only, H_2O vapor and 3000psi- SCCO_2 treatment.

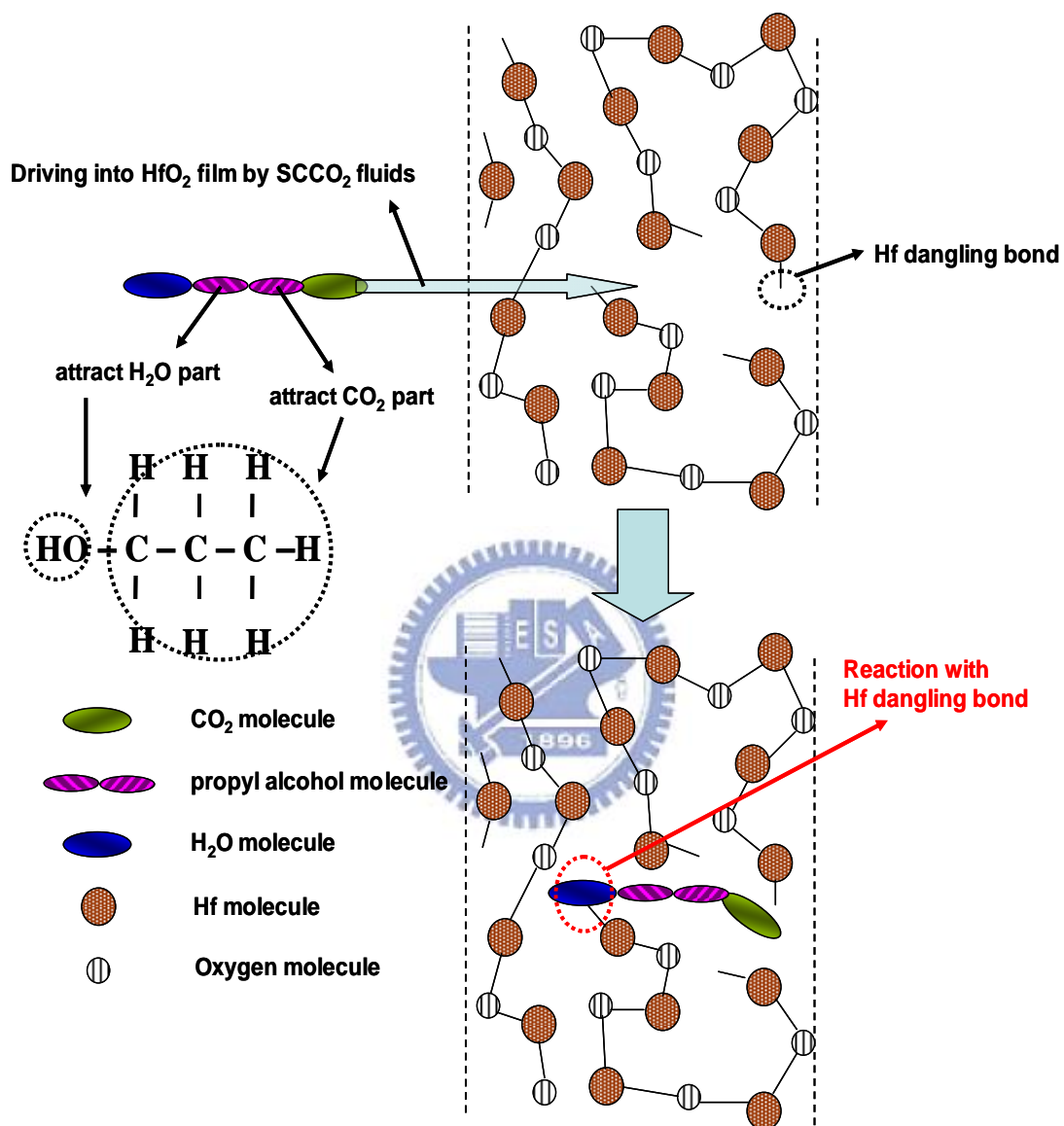


Fig. 3-12 The transporting mechanism for SCCO_2 fluids taking H_2O molecule into HfO_2 film.

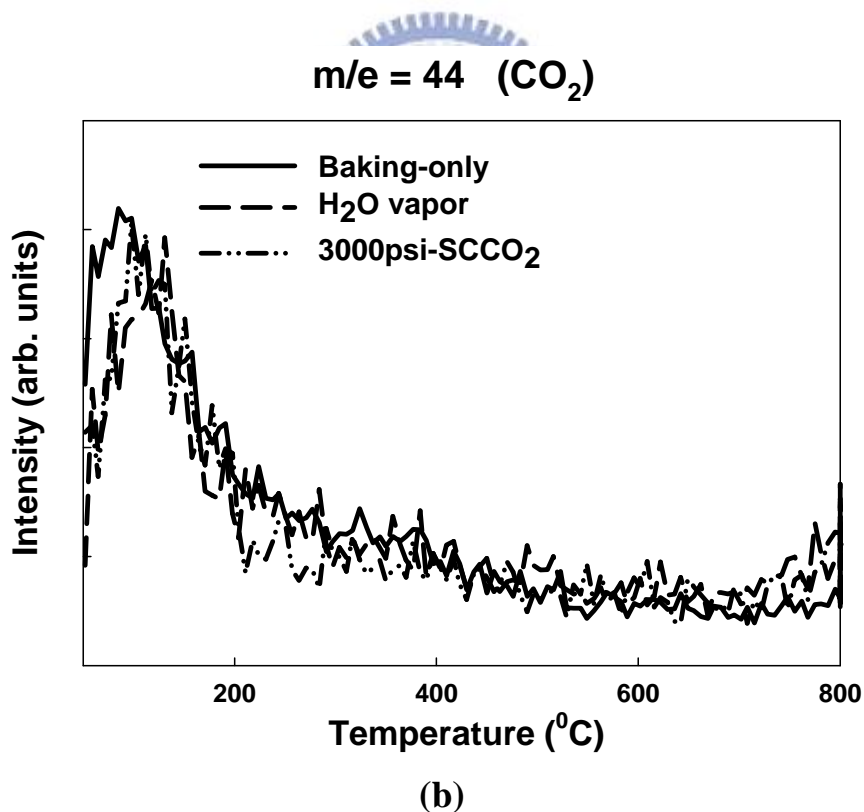
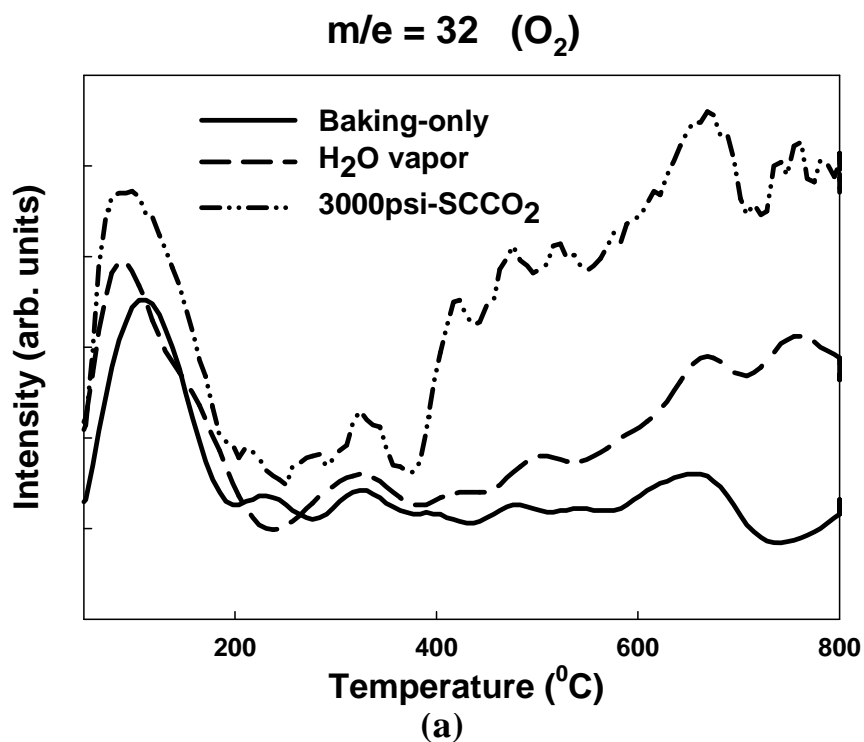


Fig. 3-13 The thermal desorption spectroscopy (TDS) measurement, (a) m/e (mass-to-charge ratio) = 32 peak that is attributed to O_2 , (b) $m/e = 18$ peak that is attributed to CO_2 .

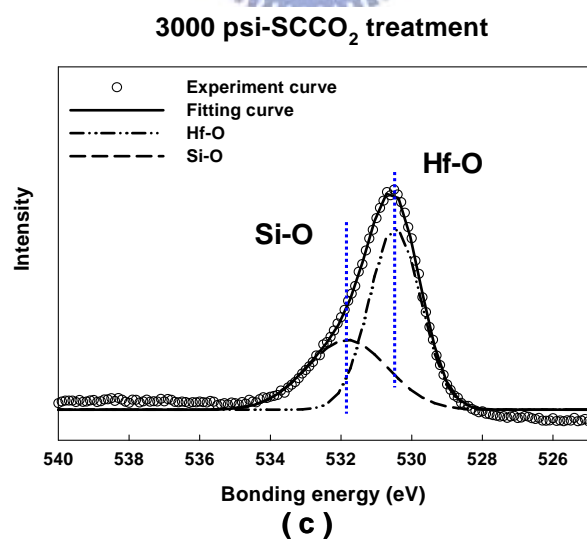
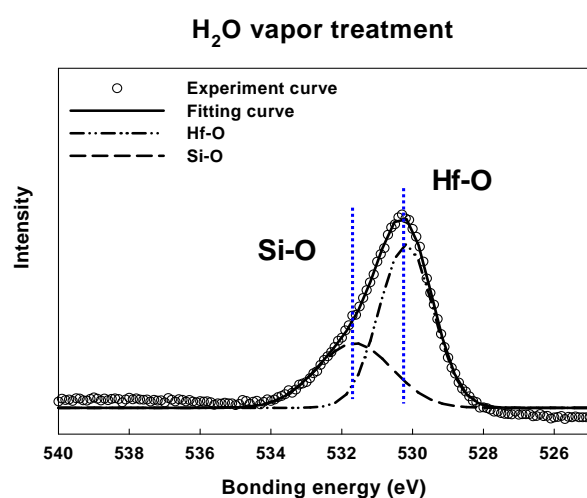
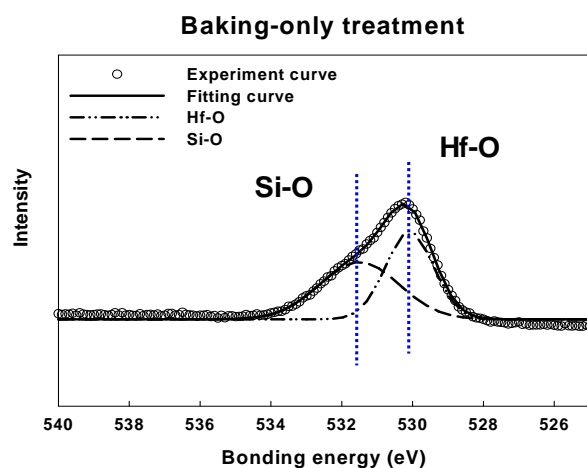


Fig. 3-14 The X-ray photoemission spectra of HfO₂ films O 1s after various post-treatments, including (a) Baking-only, (b) H₂O vapor and (c) 3000psi-SCCO₂ treatment.

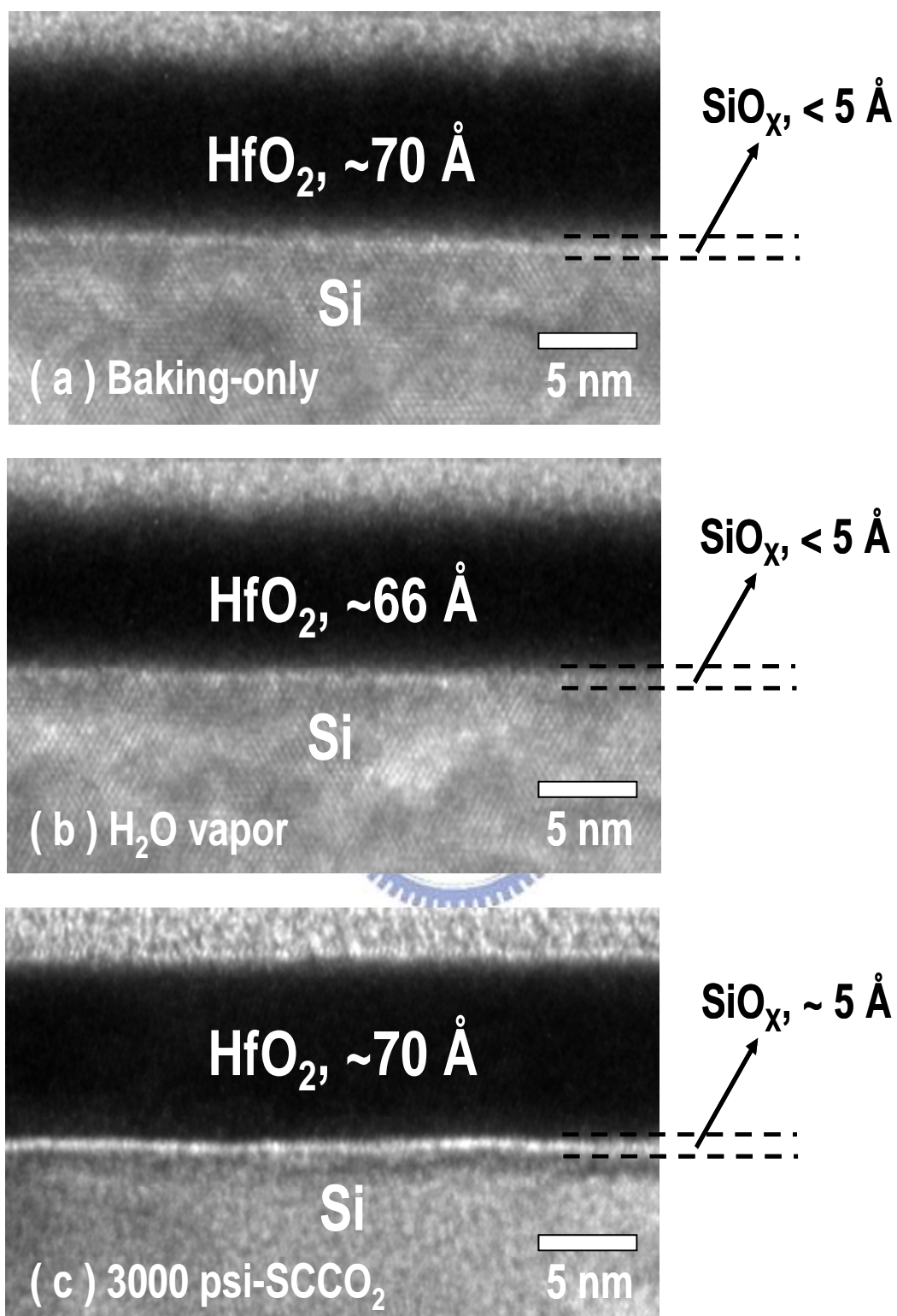


Fig. 3-15 The TEM images show the MIS (Al/HfO₂/Si-Substrate) structure after various post-treatments: (a) Baking-only treatment (b) H₂O vapor treatment and (c) 3000psi-SCCO₂ treatment.

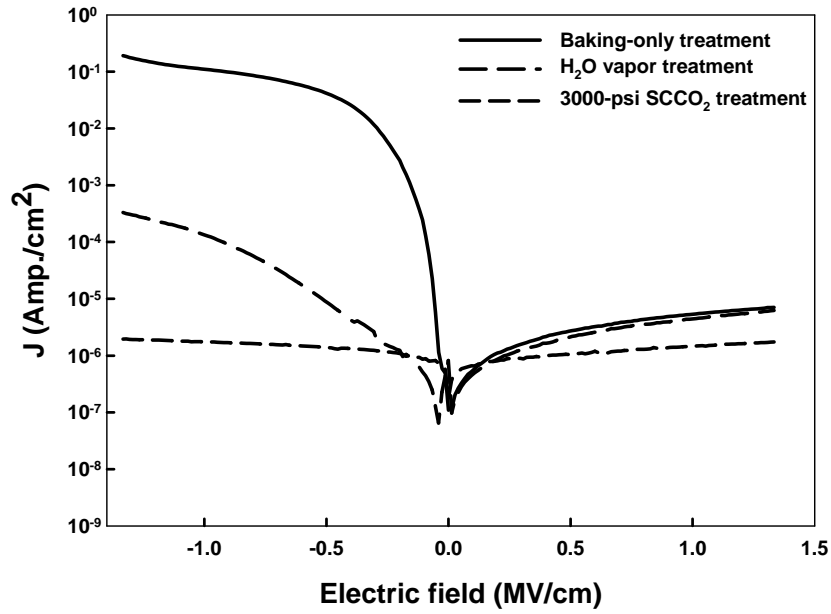


Fig. 3-16 The leakage current densities of HfO₂ films after different treatments

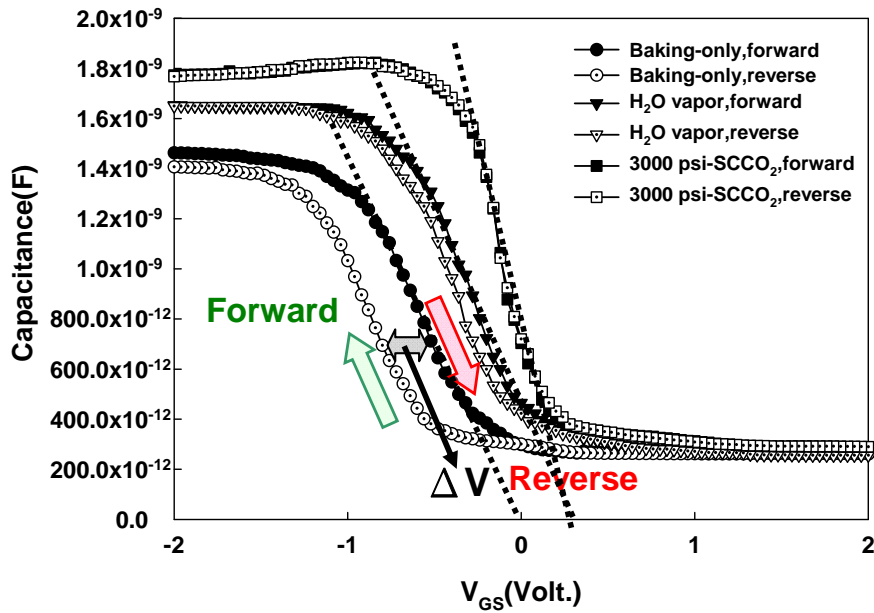
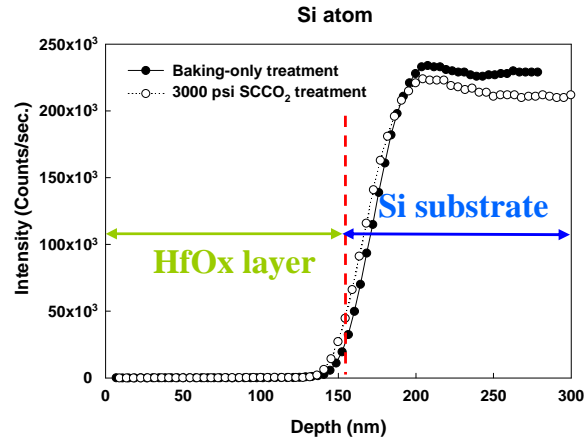
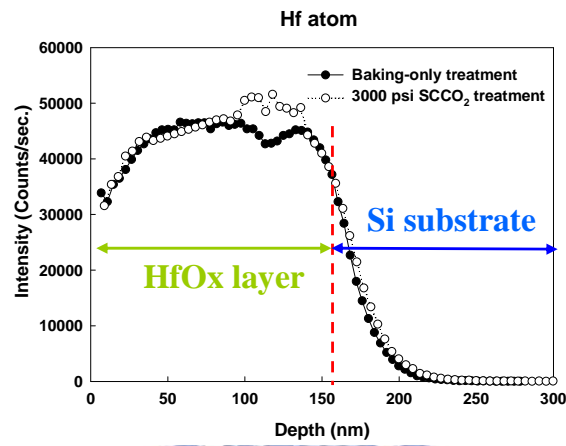


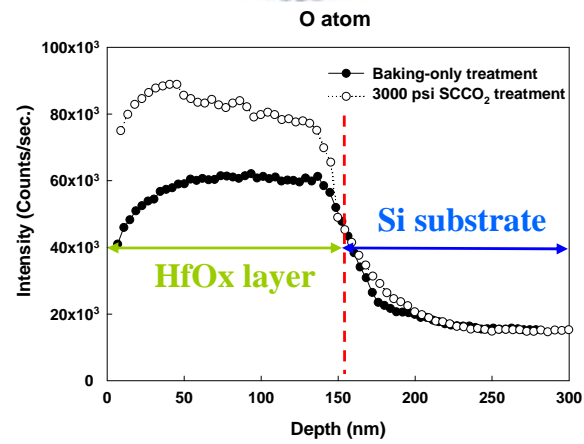
Fig. 3-17 The capacitance-voltage characteristics of HfO₂ films after different treatment, measuring at 1M Hz with gate bias swing from negative voltage to positive voltage (forward) and from positive voltage to negative voltage (reverse)



(a)



(b)



(c)

Fig. 3-17 Secondary ion mass spectroscopy: (a) Si atom (b) Hf atom and (c) O atom in HfO₂ film of Baking-only and 3000 psi-SCCO₂ treatment .

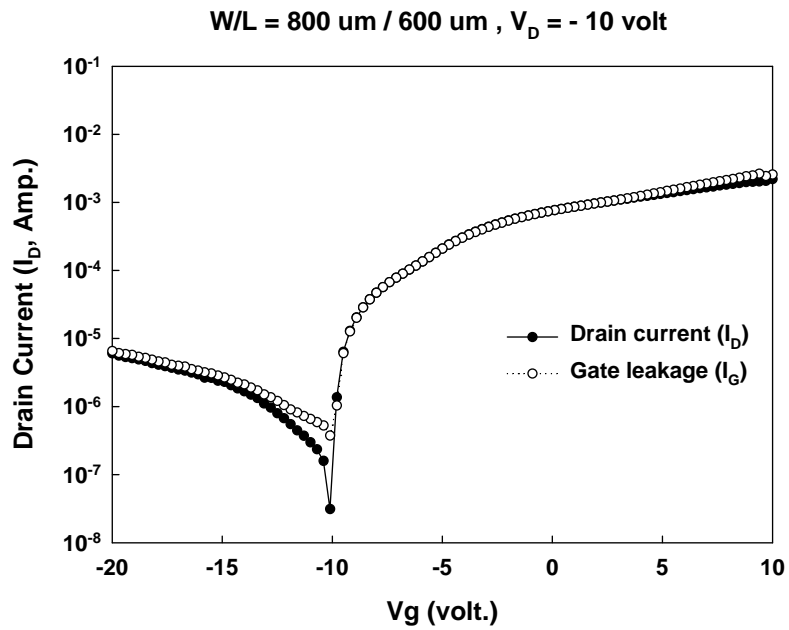
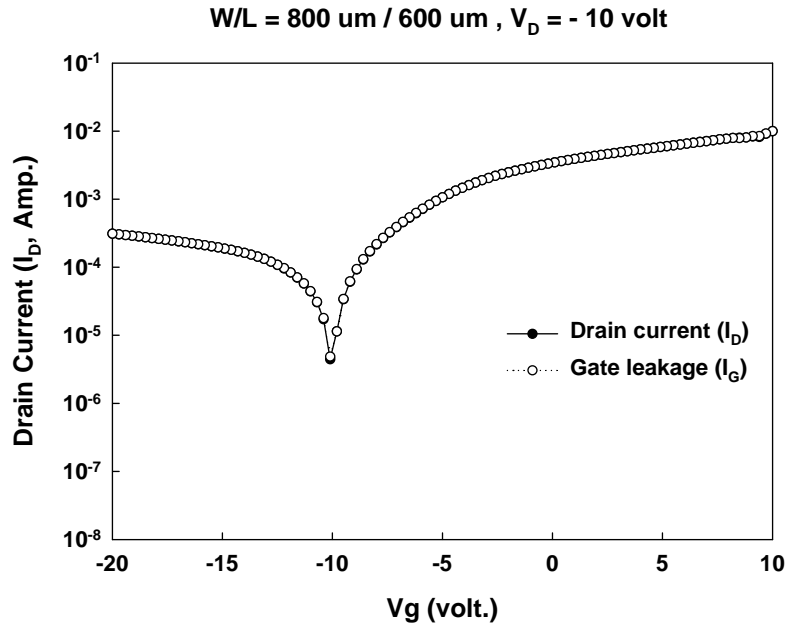


Fig. 3-18 Current vs Voltage plots (I_D - V_G) of OTFTs characteristics on HfO_2 film: (a) Baking-only treatment and (b) H_2O vapor treatment.

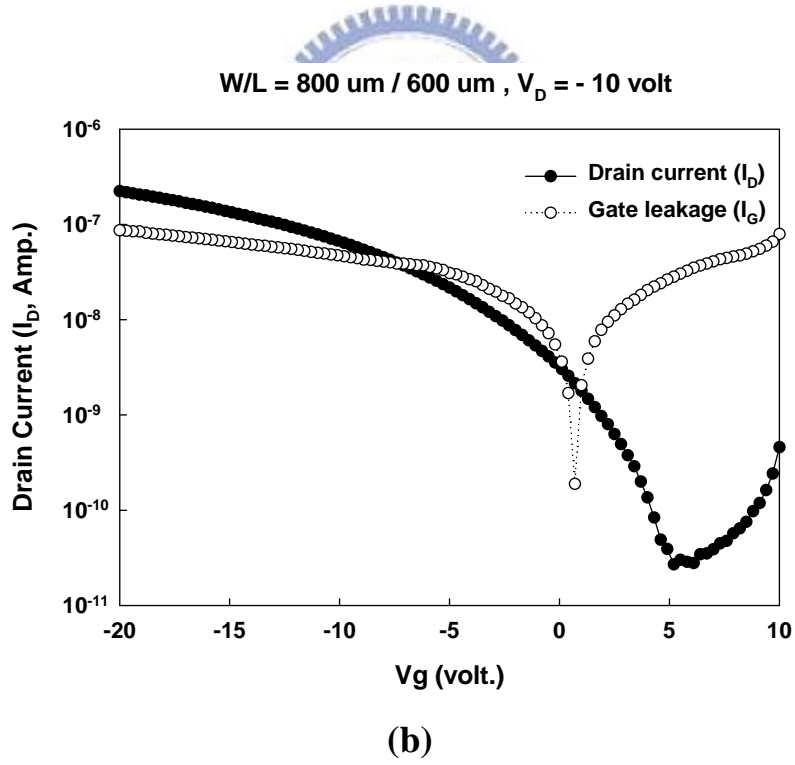
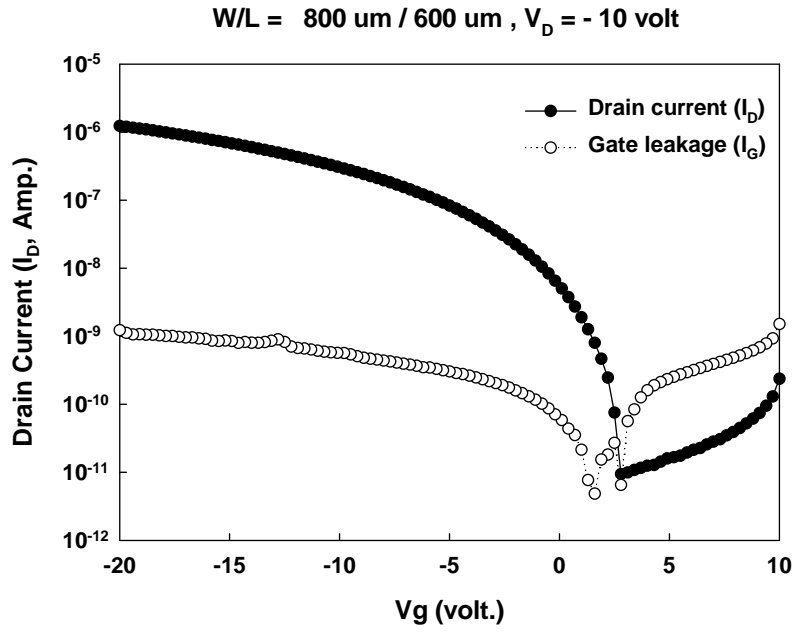


Fig. 3-19 Current vs Voltage plots (I_D - V_G) of OTFTs characteristics: (a) HfO_2 film of 3000 psi- SCCO_2 treatment and (b) PECVD SiO_2 film.

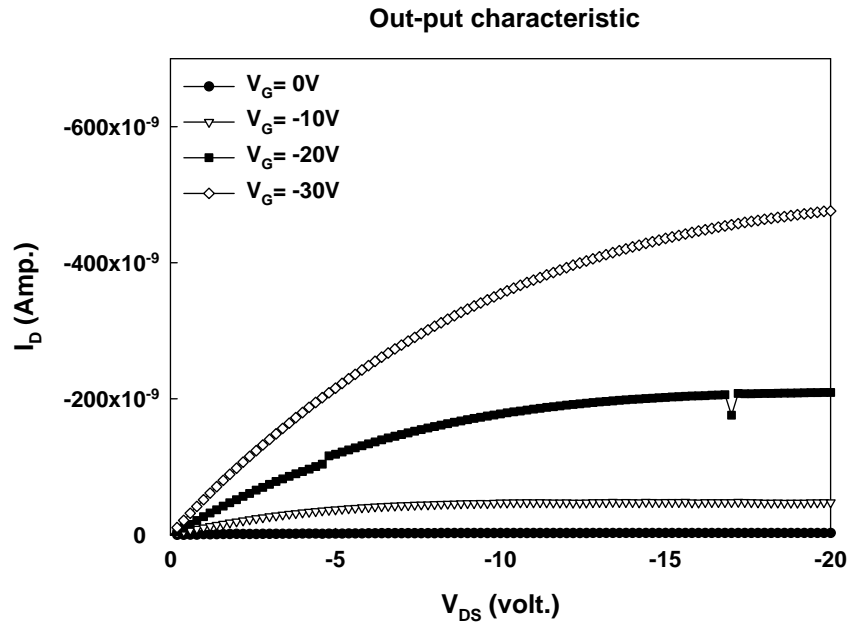
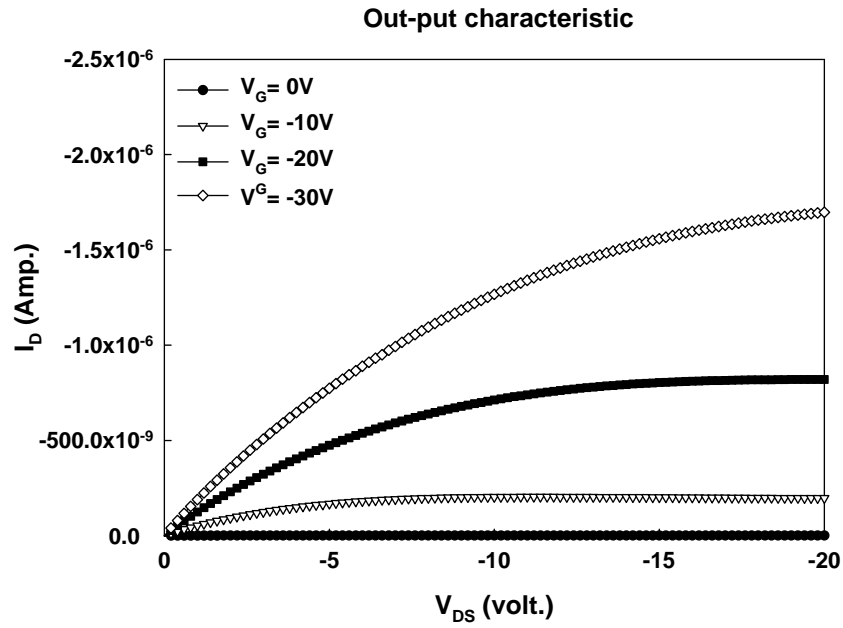


Fig. 3-20 Current vs Voltage plots (I_D - V_D) of OTFTs characteristics: (a) HfO_2 film with 3000 psi- SCCO_2 treatment and (b) PECVD SiO_2 film.

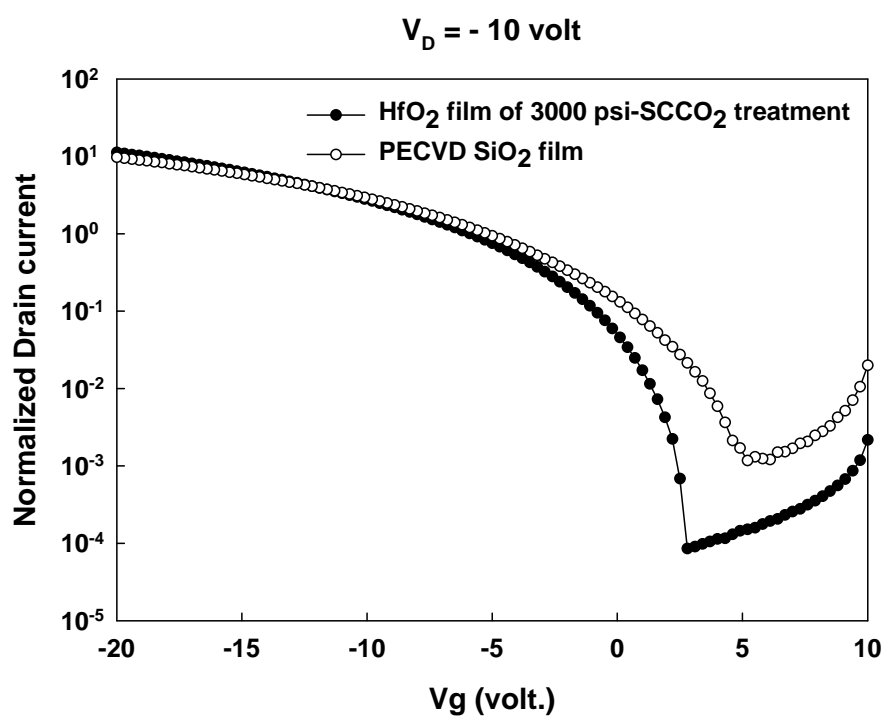


Fig. 3-21 Normalized Current vs Voltage plots (I_D - V_D) of OTFTs characteristics of HfO₂ film with 3000 psi-SCCO₂ treatment and PECVD SiO₂ film.

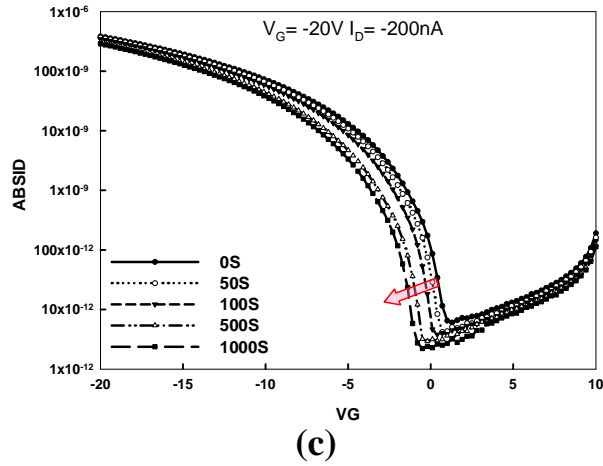
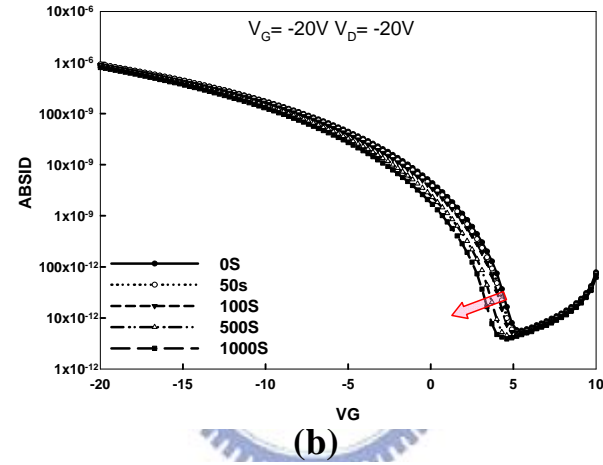
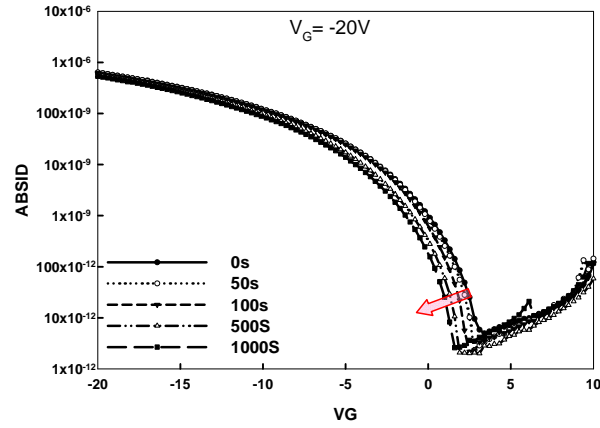


Fig. 3-22 Current vs Voltage (I_G - V_D) characteristics of a OTFTs deposited on HfO₂ film with 3000 psi-SCCO₂ treatment : (a) DC bias stress of $V_G = -20V$, (b) DC bias stress of $V_G = -20V$ and $V_D = -20V$ and (c) DC bias stress of $V_G = -20V$ and current stress of $V_D = -200nA$

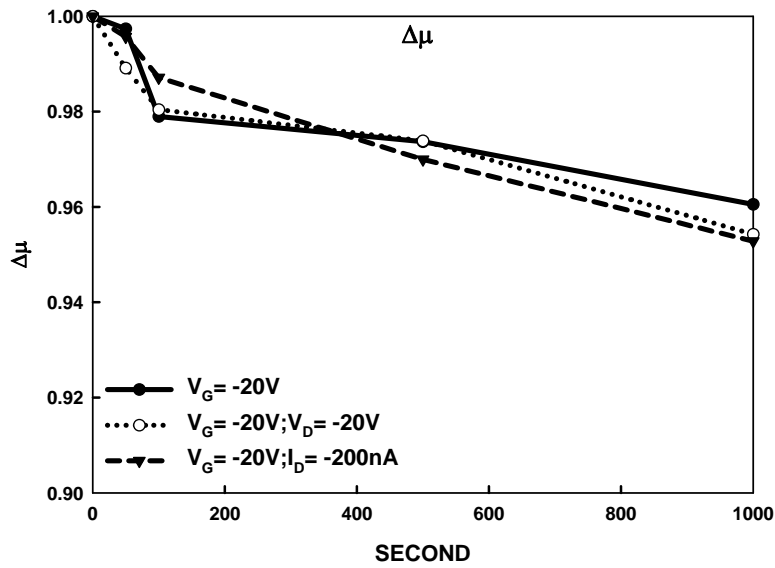


Fig. 3-23 Mobility shift vs. bias stress time for DC bias stress of $V_G = -20V$, DC bias stress of $V_G = -20V$ and $V_D = -20V$ and DC bias stress of $V_G = -20V$ and current stress of $V_D = -200nA$ (OTFTs deposited on HfO_2 film with 3000 psi-SCCO₂ treatment)

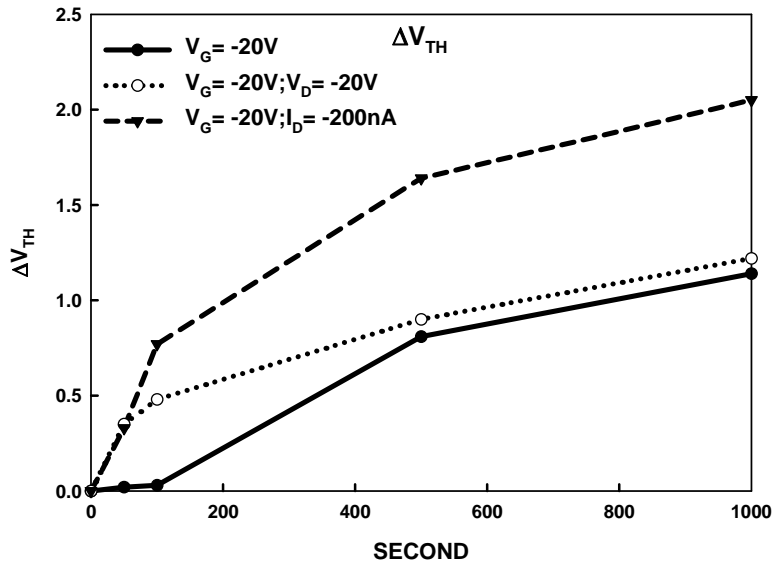
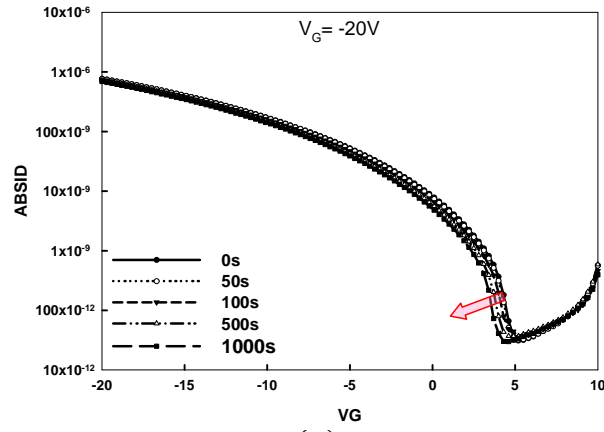
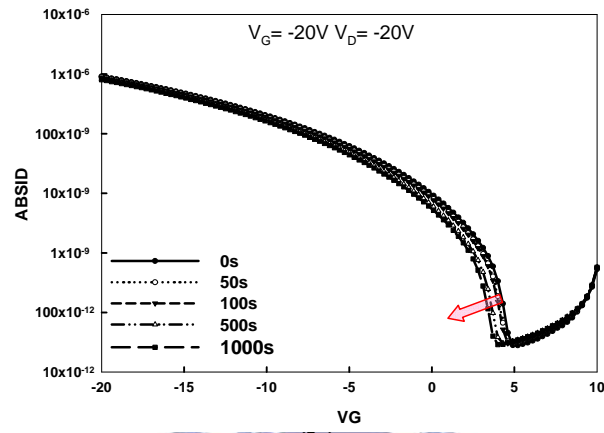


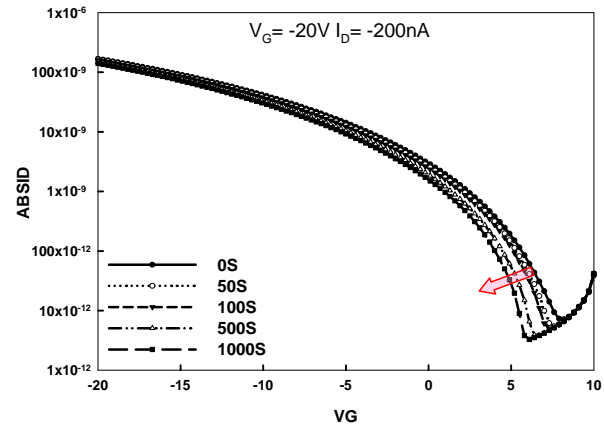
Fig. 3-24 Threshold voltage shift vs. bias stress time for DC bias stress of $V_G = -20V$, DC bias stress of $V_G = -20V$ and $V_D = -20V$ and DC bias stress of $V_G = -20V$ and current stress of $V_D = -200nA$ (OTFTs deposited on HfO_2 film with 3000 psi-SCCO₂ treatment)



(a)



(b)



(c)

Fig. 3-25 Current vs Voltage (I_G - V_D) characteristics of a OTFTs deposited on PECVD SiO_2 film : (a) DC bias stress of $V_G = -20V$, (b) DC bias stress of $V_G = -20V$ and $V_D = -20V$ and (c) DC bias stress of $V_G = -20V$ and current stress of $V_D = -200nA$

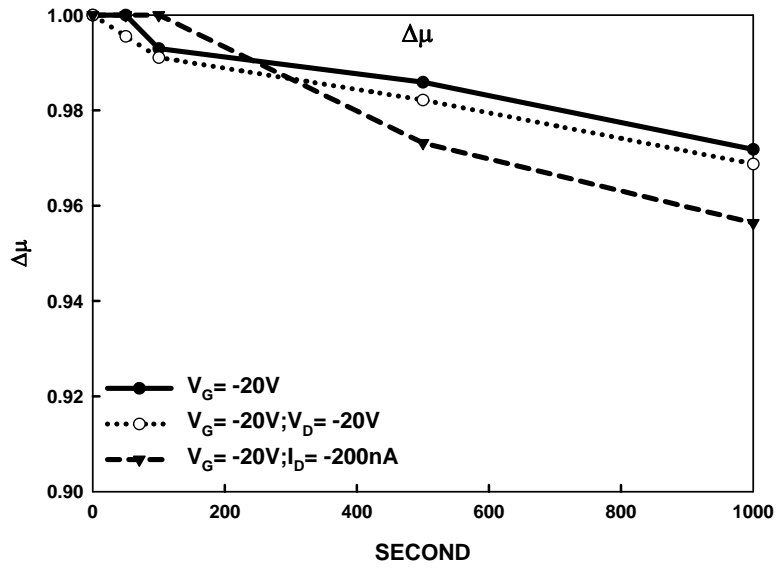


Fig. 3-26 Mobility shift vs. bias stress time for DC bias stress of $V_G = -20V$, DC bias stress of $V_G = -20V$ and $V_D = -20V$ and DC bias stress of $V_G = -20V$ and current stress of $V_D = -200nA$ (OTFTs deposited on PECVD SiO_2 film)

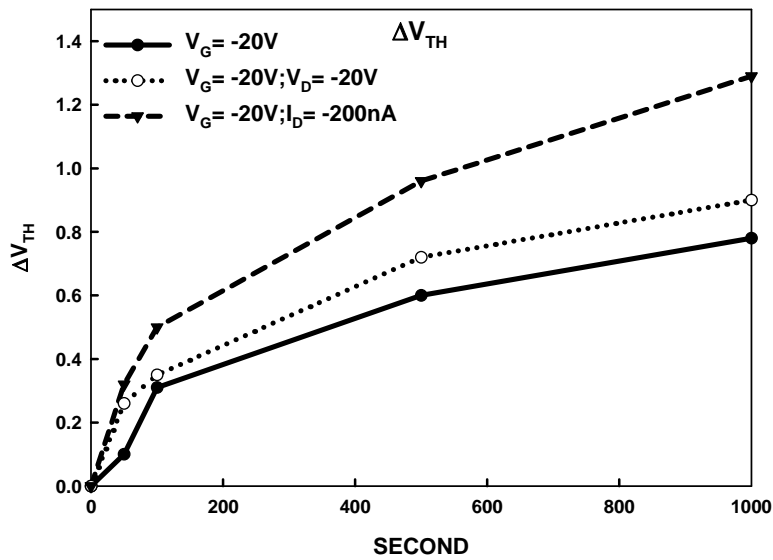


Fig. 3-27 Threshold voltage shift vs. bias stress time for DC bias stress of $V_G = -20V$, DC bias stress of $V_G = -20V$ and $V_D = -20V$ and DC bias stress of $V_G = -20V$ and current stress of $V_D = -200nA$ (OTFTs deposited on PECVD SiO_2 film)

	Baking-only	H ₂ O vapor	SCCO ₂ -3000psi
Dielectric const.	20.4	24.8	29.4
V _{0.5} (volt.), C/C _{max} = 50%	- 3.2	- 1.6	0.1
ΔV (volt.)	0.9	0.1	~ 0

Table 3-1 The extracted parameters from C-V curves of HfO₂ films after different treatment, measuring at 1M Hz with gate bias swing from negative voltage to positive voltage (forward). The V_{fb} means the flat-band voltage, and defined as C/C_{max} = 50%. The change of flat-band voltage of different- treated HfO₂ films under forward swing is label as ΔV.



References

- [1] A. Tsumura, K. Koezuka, and T. Ando, "Macromolecular electronic devices: Field-effect transistor with a polythiophene thin film", *Appl. Phys. Lett.* vol.49, pp.1210, (1986).
- [2] J. H. Burroughes, C. A. Jones, and R. H. Friend, "Polymer diodes and transistors:new semiconductor device physics", *Nature*, vol. 335, pp.137, (1988).
- [3] Y. Y. Lin, D. J. Gundlach, S. F. Nelson, and T. N. Jackson, "Pentacene organic thin-film transistors-molecular ordering and mobility", *IEEE Electron Device Lett.* vol. 18, pp. 87, (1997).
- [4] C. D. Dimitrakopoulos and P. R. L. Malenfant, "Organic thin film transistors for large area electronics", *Adv. Mater. (Weinheim, Ger.)* 14, No. 2, pp.99, (2002).
- [5] Sang Yoon Yang, Se Hyun Kim, Kwonwoo Shin, Hayoung Jeon, and Chan Eon Park, "Low-voltage pentacene field-effect transistors with ultrathin polymer gate dielectrics", *Appl. Phys. Lett.*, vol. 88, pp. 173507, (2006).
- [6] Guangming Wang, Daniel Moses, Alan J. Heeger, Hong-Mei Zhang, Mux Narasimhan, and R. E. Demaray, "Poly(3-hexylthiophene) field-effect transistors with high dielectric constant gate insulator", *J. Appl. Phys.*, vol. 95, pp. 316, (2004).
- [7] C. H. Lee, S. H. Hur, Y. C. Shin, J. H. Choi, D. G. Park, and K. Kim, "Charge-trapping device structure of SiO₂/ SiN_x/ high-k dielectric AlO_x for high-density flash memory ", *Appl. Phys. Lett.*, vol. 86, 152908, (2005).
- [8] G. D. Wilk, R. M. Wallace, and J. M. Anthony, "High- κ gate dielectrics: Current status and materials properties considerations", *J. Appl. Phys.*, vol. 89, pp. 5243, (2001).
- [9] K. Nomura, H. Ohta, K. Ueda, T. Kamiya, M. Hirano, and H. Hosono, "Thin-Film Transistor Fabricated in Single-Crystalline Transparent Oxide Semiconductor", *SCIENCE*, 300, pp. 1269, (2003).
- [10] L. A. Majewski, R. Schroeder, M. Grell, P. A. Glarvey, and M. L. Turner, "High capacitance organic field-effect transistors with modified gate insulator surface", *J. Appl. Phys.*, 96, pp. 5781, (2004).
- [11] K. Zosel, and *Angew. Chem. Engl.*, "Praktische Anwendungen der Stofftrennung mit überkritischen Gasen", *Int. Ed.* vol. 17, pp. 702, (1978).

- [12] P. M. F. Paul, and W. S. Wise, Mills&Boon, Ltd, (1971).
- [13] J. F. Brennecke, and C. A. Eckert, "Phase equilibria for supercritical fluid process design", AIChEJ, vol. 35, pp1049, (1989).
- [14] J. B. Rubin, L. B. Davenhall, C. M. V. Taylor, L. D. Sivils, T. Pierce, and K. Tiefert, "CO₂-Based Supercritical Fluids as Replacements for Photoresist-Stripping Solvents", International LANL, (1998).
- [15] L. B. Rothman, R. J. Robey, M. K. Ali, and D. J. Mount, "Supercritical fluid processes for semiconductor device fabrication", IEEE/SEMI Advanced Semiconductor manufacturing Conference, (2002).
- [16] W. H. Mullee, M. A. Biberger, and P. E. Schilling, "Removal of photoresist and residue from substrate using supercritical carbon dioxide process", United States Patent, Patent 6500605 B1, (2002).
- [17] M. Liu, Q. Fang, G. He, L. Q. Zhu, and L. D. Zhang, "Characteristics of HfON thin films by rf reactive sputtering at different deposition temperatures", J. Appl. Phys., vol. 101, 034107, (2007).
- [18] D. Brassard, D. K. Sarkar, M. A. El Khakani, and L. Ouellet, "High-*k* titanium silicate thin films grown by reactive magnetron sputtering for complementary metal-oxide-semiconductor applications", J. Vac. Sci. Technol. A, vol. 22(3), pp. 851, (2004).
- [19] Y. Ito, K. Suzulki, and R. Miura, SISPAD 2006., pp. 150, (2006).
- [20] S. Ogawa, T. Nasuno, M. Egami, and A. Nakashima, "Formation of mechanically strong low-*k* film using supercritical fluid dry technology", Interconnect Tech. Conf., Proc. of the IEEE 2002 International, pp. 220, (2002).
- [21] P. T. Liu, C. T. Tsai, T. C. Chang, K. T. Kin, P. L. Chang, C. M. Chen, and H. F. Cheng, "Activation of Carbon Nanotube Emitters by Using Supercritical Carbon Dioxide Fluids with Propyl Alcohol" Electrochem. Solid-State Lett., vol. 9(4), pp. G124, (2006).
- [22] P. T. Liu, C. T. Tsai, T. C. Chang, K. T. Kin, P. L. Chang, "Effects of Supercritical Fluids Activation on Carbon Nanotube Field Emitters", IEEE Trans. Nanotech., vol. 6, pp. 29, (2007).
- [23] M. L. Lee and K. E. Markides, "Analytical Supercritical Fluid Chromatography and Extraction.", Provo, UT: Chromatography Conferences, (1990).
- [24] Lisong Zhou, Alfred Wanga, Sheng-Chu Wu, Jie Sun, Sungkyu Park, and Thomas N. Jackson, "All-organic active matrix flexible display", Appl. Phys.

- Lett., vol. 88, 083502, (2006).
- [25] C. D. Sheraw, L. Zhou, J. R. Huang, D. J. Gundlach, and T. N. Jackson, “Organic thin-film transistor-driven polymer-dispersed liquid crystal displays on flexible polymeric substrates”, Appl. Phys. Lett., vol. 80, pp. 1088, (2002).
- [26] J. Robertson, “Interfaces and defects of high-k oxides on silicon”, Solid-State Electronics vol. 49 pp. 283, (2005).
- [27] H. Klauk, M. Halik, U. Zschieschang, G. Schmid, W. Radlik. “Polymer gate dielectric pentacene TFT and circuits on flexible substrates”, Technical Digest of IEDM, 557, (2002)
- [28] T. W. Kelley, D. V. Muryes, P. F. Baude, T. P. Smith, and T. D. Jones. “High performance of organic thin film transistors, in Organic and Polymeric Materials and Devices”, edited by P. W. M. Blom, N. C. Greenham, D. D. Dimitrakopoulos, and C. D. Frisbie. Mater. Res. Soc. Symp. Proc. 771, Warrendale, PA, P. 169,(2003)
- [29] H. Sirringhaus, P. J. Brown, R. H. Friend, M. M. Nielsen, K. Bechgaard, B. M. W. Langeveld-Voss, A. J. H. Spiering, R. A. J. Janssen, E. W. Meijer, P. Herwig, D. M. de Leeuw. “Two-dimensional charge transport in self-organized, high-mobility conjugated polymers”, Nature, Vol 401, pp 685-688 (1999)
- [30] G. M. Wang, J. Swensen, D. Moses, and A. J. Heeger, “Increased mobility from regioregular poly (3-hexylthiophene) field-effect transistors”, J. Appl. Phys, Vol 93, pp 6137, (2003)
- [31] F. Ebisawa, T. Kurosawa, S. Nara, “Electrical properties of Polycarbonate/polysiloxane interface”, J. Appl. Phys, Vol. 54, pp. 3255-3259, (1983)
- [32] L. Sebastian, G. Weiser, and H. Bassler, “Charge transfer transitions in solid tetracene and pentacene studied by electroabsorption”, Chemical Physics, Vol 61, pp 125-135, (1981)
- [33] S. F. Nelson, Y.-Y. Lin, D. J. Gundlach, and T. N. Jackson, “Temperature-independent transport in high-mobility pentacene transistors”, Appl. Phys. Lett., Vol. 72, pp.1854 (1998)
- [34] E. A. Silinsh, and V. Capek, “Organic Molecular Crystals: Their Electronic States”, New York, (1980)
- [35] T. Torsi, “Novel applications of organic based thin film transistors”, Solid-State Electronics, Vol 45, pp 1479-1485, (2001)

- [36] G. Horowitz, R. Hajlaoui, P. Delannoy, "Temperature dependence of the field-effect mobility of sexithiophene. Determination of the trap density", *J-Phys III France* 5:355-371, (1995)
- [37] W. E. Spear and P. G. Le Comber, *J. Non-Cryst. Solids* 8-10, 727 (1972)
- [38] C. D. Dimitrakopoulos, S. Purushothaman, J. Kymissis, A. Callefari, J. M. Shaw, "Low-voltage organic transistors on plastic comprising high-dielectric-constant gate insulator", *Science*, Vol 283, pp 822-824, (1999)
- [39] C. D. Dimitrakopoulos, J. Kymissis, S. Purushothaman, D. A. Neumayer, P. R. Duncombe, R. B. Laibowitz, "Low-voltage, high-mobility pentacene transistors with solution-processed high-dielectric constant insulators", *Adv. Mater*, Vol 11: 1372-1375, (1999)
- [40] I. Muzicante, E. A. Silinsh. "Investigation of local trapping states in organic molecular crystals by method of thermally modulated space-charge limited current. *Acta.Phys Pol A (Poland)* 88:389-399, (1995)
- [41] N. Karl, "Getting beyond impurity-limited transport in organic photoconductors. In K. Sumino, ed, "Defect Control in Semiconductors. Vol. II. Amsterdam : North Holland, pp 1725-1746, (1999)
- [42] G. Horowitz, M. E. Hajlaoui, "Mobility in polycrystalline oligothiophene field-effect transistors dependent on grain size", *Adv. Mater*, Vol 12, pp 1046-1050, (2000)
- [43] G. Horowitz, M. E. Hajlaoui, R. Hajlaoui, "Temperature and gate voltage dependence of hol mobility in polycrystalline oligothiophene thin-film transistors", *J. Appl. Phys*, Vol 87, pp 4456-4463, (2000)
- [44] E. A. Silinsh, A. Klimkans, S. Larsson, and V. Capek, "Molecular polaron states in polyacene crystals. Formation and transfer processes", *Chem. Phys*, Vol 198, pp 311, (1995)
- [45] M. D. J. M. Vissenberg, M. Matters, "Theory of the field-effect mobility in amorphous organic transistors", *Phys. Rev. B*, Vol 57, pp 12964, (1998)
- [46] M. Halik, H. Klauk, U. Zscieschang, G. Shmid, C. Dehm, M. Schutz, S. Maisch, F. Effeberger, M. Brunnbauer, and F. Stellacci, "Low-voltage organic transistors with an amorphous molecular gate dielectric", *Nature*, Vol 43, pp 963-966, (2005)

- [47] W. J. Zhu, Tso-Ping Ma, Takashi Tamagawa, J. Kim, and Y. Di, "Current transport in metal/hafnium oxide/silicon structure", IEEE Electron Devices Lett. vol. 23, No. 2, (2002).
- [48] Takeshi Yamaguchi, Hideki Satake, and Noburu Fukushima, "Band diagram and carrier conduction mechanisms in ZrO₂/sub 2/MIS structures", IEEE Trans. Electron Devices, vol. 51, No. 5, (2004).
- [49] M. Houssa, M. Tuominen, et al., "Trap-assisted tunneling in high permittivity gate dielectric stacks", J. Appl. Phys., vol. 87, No. 12, pp. 8615, (2000).
- [50] Sanghun Jeon, Hyundoek Yang, Dae-Gyu Park, and Hyunsang Hwang, "Electrical and Structural Properties of Nanolaminate (Al₂O₃/ZrO₂/Al₂O₃) for Metal Oxide Semiconductor Gate Dielectric Applications", Jpn. J. Appl. Phys., vol. 31, pp. 2390-2393, (2002).
- [51] Dieter K. Schroder, Wiley-INTERSCIENCE, (1998).
- [52] M. Lenzlinger, and E. H. Snow, "Fowler-Nordheim tunnelling into thermally grown SiO₂", J. Appl. Phys., vol. 40, pp. 278, (1969).
- [53] R. Mahapatra, A. K. Chakraborty, N. Poolamai, A. Horsfall, S. Chattopadhyay, and N. G. Wright, "Leakage current and charge trapping behavior in TiO₂/SiO₂ high- κ gate dielectric stack on 4H-SiC substrate", J. Vac. Sci. Technol. B, vol. 25(1), pp. 217, (2007).
- [54] P. R. Emtage, and W. Tantraporn, "Schottky Emission Through Thin Insulating Films", Phys. Rev. Lett., vol. 8, pp. 267, (1962).
- [55] J. R. Yeargan, and H. L. Taylor, "Conduction Properties of Pyrolytic Silicon Nitride Films", J. Appl. Phys., vol. 39, pp. 5600, (1968).
- [56] S. W. Huang, and J. G. Hwu, "Electrical characterization and process control of cost-effective high- κ aluminum oxide gate dielectrics prepared by anodization followed by furnace annealing", IEEE Trans. Electron Devices, vol. 50, pp. 1658, (2003).
- [57] T. FUKUDA, and H. YANAZAWA, "A Novel Method of Removing Impurities from Multilevel Interconnect Materials", Jpn. J. Appl. Phys., vol. 43, pp. 936, (2004).
- [58] F. Crupi, R. Degraeve, A. Kerber, D. H. Kwak, and G. Groeseneken, "Correlation between stress-induced leakage current (SILC) and the HfO₂ bulk trap density in a SiO₂/HfO₂ stack", IEEE 42nd 70 Annual International

- Reliability Physics Symposium, pp. 181, (2004)
- [59] H.Y. Yu, X.D. Feng, D. Grozea, Z.H. Lu, R.N.S. Sodhi, A.M. Hor, H. Aziz, "Surface electronic structure of plasma-treated indium tin oxides" *Appl. Phys. Lett.* 78, 2595, (2001).
- [60] J.P. Chang, Y.S. Lin, "Highly conformal ZrO₂ deposition for dynamic random access memory application" *J. Appl. Phys.* 90, 2964, (2001).
- [61] A. Benninghoven, F. G. Rudenauer and H. W. Werner, "Secondary Ion Mass Spectrometry," (Wiley, New York) p.1227, (1987).

